

**AN ULTRA-COMPACT AND LOW LOSS PASSIVE
BEAMFORMING NETWORK INTEGRATED ON CHIP WITH OFF
CHIP LINEAR ARRAY**

A Thesis
Presented to
The Academic Faculty

by

Stefan Lepkowski

In Partial Fulfillment
of the Requirements for the Degree
Master's in the
School of Electrical and Computer Engineering

Georgia Institute of Technology
May 2015

[COPYRIGHT© 2015 BY STEFAN LEPKOWSKI]

**AN ULTRA-COMPACT AND LOW LOSS PASSIVE
BEAMFORMING NETWORK INTEGRATED ON CHIP WITH OFF
CHIP LINEAR ARRAY**

Approved by:

Dr. Hua Wang, Advisor
School of Electrical and Computer Engineering
Georgia Institute of Technology

Dr. John Papapolymerou
School of Electrical and Computer Engineering
Georgia Institute of Technology

Dr. Muhannad Bakir
School of Electrical and Computer Engineering
Georgia Institute of Technology

Date Approved: 4/21/2015

ACKNOWLEDGEMENTS

I would like to thank my parents for their continued support of my education. Also, the members of the GEMS group at Georgia Tech for their patience and assistance. Their help has been invaluable. Lastly, Dr. Hua Wang for allowing me to join his lab. In doing so, it gave me the opportunity to learn alongside the best and brightest.

TABLE OF CONTENTS

	Page
ACKNOWLEDGEMENTS	iii
LIST OF TABLES	vi
LIST OF FIGURES	vii
SUMMARY	x
 <u>CHAPTER</u>	
1 Introduction	1
The Butler Matrix	4
2 Theory	7
Transformer Based Quadrature Coupler	15
Phase Shifter	21
Antenna Array	24
3 Butler Matrix Design	27
Technology	27
Validation	28
EM Model Layout	31
Design for Test	34
Antenna Array	36
Flip Chip Bonding	39
Antenna Feed Lines	42
Antenna Array	43
4 Simulation Results	46
5 Conclusion and Future Work	55

Appendix A	57
Combined Radiation Patterns	57
REFERENCES	61

LIST OF TABLES

	Page
Table 1. Phase shifter comparison at 60 GHz.	33
Table 2. Transistor Equivalent Impedance	38
Table 3. Peak to Null Ratio for Excited Beams	47
Table 4. Performance Comparison	48
Table 5. Simulated electrically synthesized beam and antenna pattern performance.	49
Table 6. Array performance with multiple excitations	50

LIST OF FIGURES

	Page
Figure 1. Using beam forming for spatial filtering.	2
Figure 2. Linear antenna array showing variable definitions.	3
Figure 3. Ideal antenna array performance showing the normalized main lobe and relative side lobe levels for an 8 element $\lambda/2$ array.	4
Figure 4. Electrically synthesized beam pattern for and 8x8 Butler Matrix	5
Figure 5. Coupler symbol and the branch line phase relations <i>between</i> the <i>Thru</i> and <i>Coupled</i> ports when <i>excited</i> from <i>Input</i> .	7
Figure 6. Degraded quadrature phase balance.	8
Figure 7. A 4x4 Butler Matrix topology excluding the antenna crossover.	9
Figure 8. Phase relations when exciting the 4x4 Butler Matrix from port 1.	10
Figure 9. Modular coupler phase used to generate an 8x8 Butler Matrix's phase differences	11
Figure 10. The 8x8 Butler Matrix using transformer-based couplers	12
Figure 11. Ideal electrically synthesized beam 1R (port 1) of the swapped port 8x8 Butler Matrix.	14
Figure 12. Amplitude and phase error are responsible for an error vector and degrade PNR performance.	15
Figure 13. Partial compensation of coupler phase error with phase shifter.	18
Figure 14. EM structure of the transformer based coupler.	20
Figure 15. Amplitude balance comparison of the branch line and transformer based coupler.	20
Figure 16. Input matching comparison of the branch line and transformer based coupler.	21
Figure 17. Phase balance comparison of branch line and transformer based coupler.	21
Figure 18. C-L-C π -network circuit.	22
Figure 19. Array factor for an 8 element linear uniform amplitude and uniform spaced array.	25

Figure 20. Signal distribution of combined excitations and ideal cosine distribution of antenna elements.	26
Figure 21. Metal layer stackup for the 65nm Bulk CMOS process.	28
Figure 22. Imported GDSII stream file from Cadence® used to validate stackup.	29
Figure 23. Two load conditions to determine transmission line characteristic impedance.	30
Figure 24. First phase matching stage showing minimum phase path (red), 22.5° path (yellow) and 67.5° path (green).	32
Figure 25. Phase matching quality of the different paths.	32
Figure 26. Loss comparison of different paths.	33
Figure 27. Second stage phase matching stage with 0° paths (green) and 45° paths.	34
Figure 28. Stepped impedance filter as a crossover.	35
Figure 29. HFSS® EM final metal layout structure and core dimensions.	36
Figure 30. Testing setup showing the termination limitation of probes.	37
Figure 31. Equivalent model for the termination transistors.	38
Figure 32. Equivalent termination transistor model at the edge of the ground plane.	38
Figure 33. Effects of transistor in output matching.	39
Figure 34. Flip chip wire bond side view used between Butler Matrix and antenna array.	40
Figure 35. Flip chip wire bonds between silicon IC and antenna substrate.	41
Figure 36. Flip chip matching between the silicon IC and antenna feed lines.	41
Figure 37. Insertion loss of the flip chip bonds.	42
Figure 38. EM model for the antenna feed structure.	43
Figure 39. Single slot dipole and associated dimensions.	44
Figure 40. 8 element linear array.	45
Figure 41. Simulated electrically synthesized beam pattern.	46
Figure 42. Simulated PNR vs. frequency.	47

Figure 43. Slot dipole radiation pattern.	49
Figure 44. Normalized simulated beam pattern of excitation 4L.	51
Figure 45. Normalized simulated beam pattern of excitation 3L.	51
Figure 46. Normalized simulated beam pattern of excitation 2L.	52
Figure 47. Normalized simulated beam pattern of excitation 1L.	52
Figure 48. Normalized simulated beam pattern of excitation 1R.	53
Figure 49. Normalized simulated beam pattern of excitation 2R.	53
Figure 50. Normalized simulated beam pattern of excitation 3R.	54
Figure 51. Normalized simulated beam pattern of excitation 4R.	54
Figure 52. 4R and 3R excitation.	57
Figure 53. 3R and 2R excitation.	57
Figure 54. 2R and 1R excitation.	58
Figure 55. 1R and 1L excitation.	58
Figure 56. 1R and 2R excitation.	59
Figure 57. 2R and 3R excitation.	59
Figure 58. 3R and 4R excitation.	60

SUMMARY

The work here presents a review of beam forming architectures. As an example, the author presents an 8x8 Butler Matrix passive beam forming network including the schematic, design/modeling, operation, and simulated results. The limiting factor in traditional beam formers has been the large size dictated by transmission line based couplers. By replacing these couplers with transformer-based couplers, the matrix size is reduced substantially allowing for on chip compact integration. In the example presented, the core area, including the antenna crossover, measures 0.82mm×0.39mm (0.48% the size of a branch line coupler at the same frequency). The simulated beam forming achieves a peak PNR of 17.1 dB and 15dB from 57 to 63GHz. At the 60GHz center frequency the average insertion loss is simulated to be 3.26dB. The 8x8 Butler Matrix feeds into an 8-element antenna array to show the array patterns with single beam and adjacent beam isolation.

Chapter 1

Introduction

Beam forming is a method of spatial power combining based on the application of signals to antenna arrays. By controlling the relative phase and/or amplitude, signals are combined or cancelled to create focused radiation patterns. In defense applications, beam formers are found in applications such as phased array radar systems, microwave/mm-wave imaging systems, jammers and jammer tolerant receivers in electronic warfare (EW) [1]-[4]. In the commercial sector, beam formers are being explored for use in MIMO cell systems and mm-wave high-speed wireless HD data link [5]-[9].

In applications such as radar systems beam formers provide target location information from reflected signals (Figure 1). If a signal is reflected by a target while a beam is excited in a certain direction, the target is known to lie in the direction the beam was formed. Simultaneously, reflected signals outside the main lobe are attenuated, this effect is also spatial filtering. It is desirable in application to increase the antenna gain or directivity. This can be achieved through an increased number of antenna elements.

The simplest beam formers use linear antenna array configurations with uniform amplitude and phase differences. The plane waves produced by the network at different phases are superimposed in the far field to increase directivity and gain. The scan angle of the array is based on the phase difference between elements and the physical separation. The disadvantage of a linear array is the fixed side lobe level when using uniform element spacing and equal amplitude signals, which can be mitigated by signal

amplitude tapering, or unequal element spacing. The antenna array side lobes can cause power to be directed in an unintended manner. These side lobe levels can cause the unwanted effect of creating false positives when scanning a specific area in space, where even though no targets may lie in the direction of the main beam, the power transmitted and reflected in the lobes may be enough to trigger a detection.

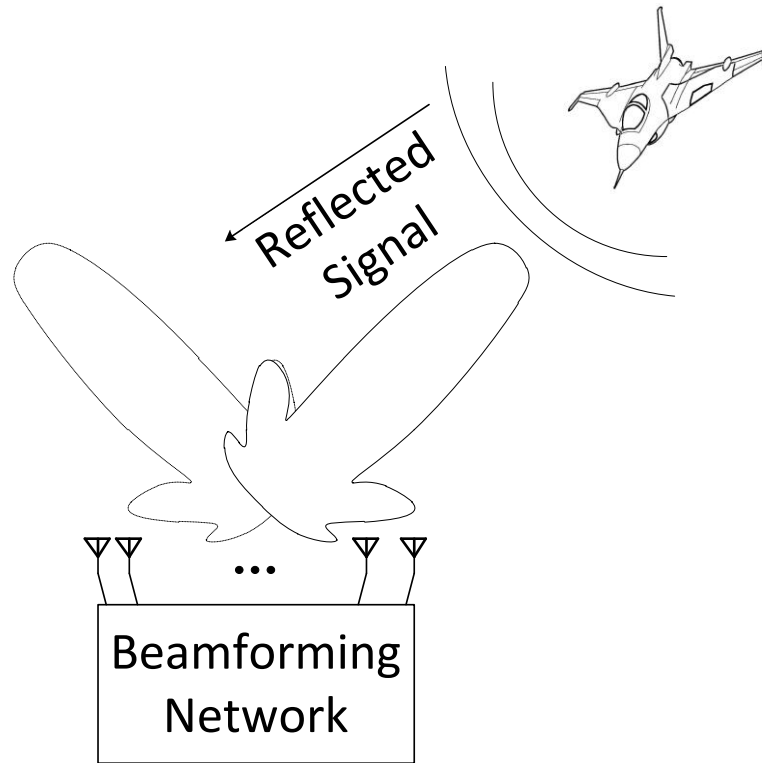


Figure 1. Using beam forming for spatial filtering.

If we array a series of antennas with an isotropic array pattern, the radiation pattern will be determined by the array factor of the configuration.

$$\textit{Combined Pattern} = \textit{Array Factor} \times \textit{Single Element Pattern}$$

This array factor is a function of the spacing, phase, and amplitude weighting of the fields being combined. Figure 2 shows the linear array configuration aligned along the y-axis with θ being measured from the broadside to the array.

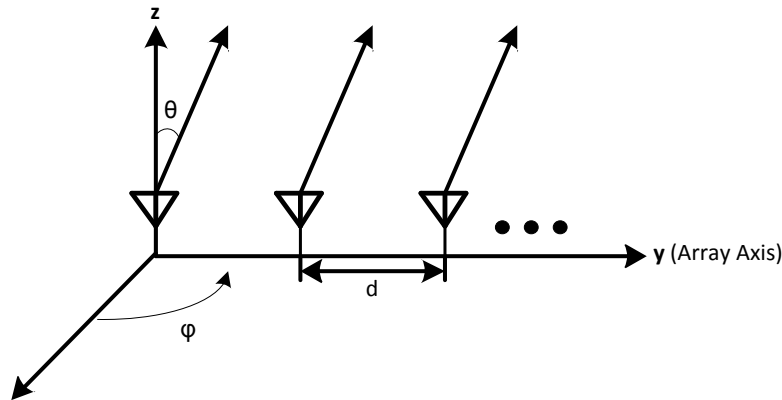


Figure 2. Linear antenna array showing variable definitions.

An example scan angle, 0° , for the linear array is shown below, Figure 3. In creating the beam pattern for an array it has been assumed that each element radiates isotropically. Therefore, when the array factor is multiplied by the directivity of the individual antenna the array factor is not modified. It is seen that by using multiple elements, the pattern is focused into a beam with a series of lower relative power side lobes. These side lobes can be responsible for out of beam interferences and, as mentioned above, for triggering false positives. The side lobe level (SLL) is a measure of rejection between the main beam and the side lobe. Figure 3 is the array factor for an 8-element uniform amplitude, $\lambda/2$ uniform spacing.

Although Figure 3 shows the pattern for a broadside excitation using a 0° phase difference between array elements, the beam can be steered by introducing a phase

difference between array elements. Generating phase differences is the duty of the beam forming network.

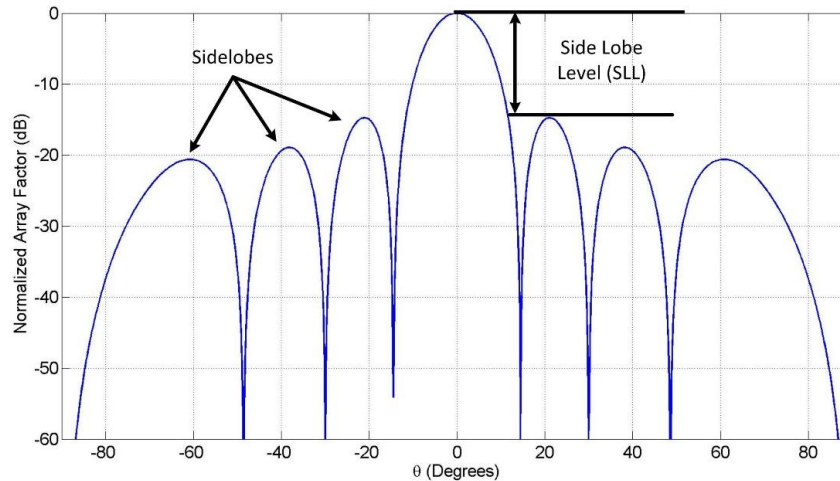


Figure 3. Ideal antenna array performance showing the normalized main lobe and relative side lobe levels for an 8 element $\lambda/2$ array.

The Butler Matrix

An example beam forming network, presented here, is called a “Butler Matrix”, named after of one the individuals credited with its development, Jesse Butler [1]. A Butler Matrix is a method of passive and multi-beam forming in which an input to the Butler Matrix generates a beam in a fixed direction. In comparison to active beam forming, passive beam forming is achieved without DC power consumption or dynamic tunability. The Butler Matrix is responsible for providing the phase differences to the antenna array. A characteristic output from a 3rd order Butler Matrix, i.e. 8x8, is presented below in Figure 4. The reader will note, there are 8 traces placed on the same plot. Each of these traces represents a unique beam corresponding to an input port of the Butler Matrix.

The core component of the Butler Matrix is the 90° quadrature coupler. The coupler is responsible for dividing and recombining signals passing through the matrix. It must maintain amplitude and phase balance as well as adjacent port isolation in order for proper operation of the Butler Matrix. Additionally, impedance matching is required for network elements to be cascaded without ill effect.

A metric used here to gauge the performance of the Butler Matrix is called the peak to null ratio. This metric is a comprehensive measure of phase and amplitude performance. It is the separation between the peak of a receive signal and rejection in the null, Figure 4. Ideally this value is infinite but as error accrues in the performance this value quickly increases.

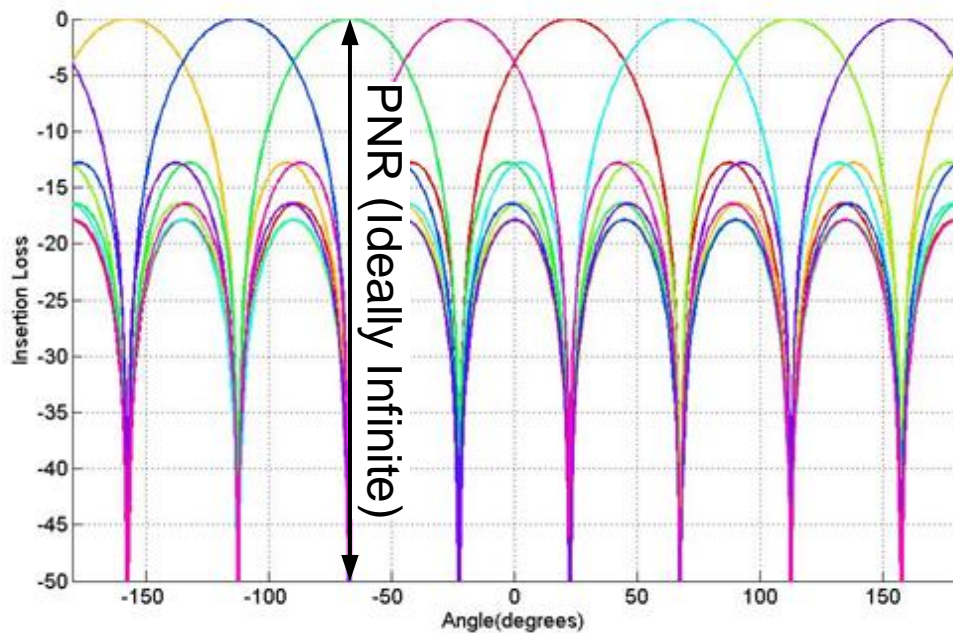


Figure 4. Electrically synthesized beam pattern for and 8x8 Butler Matrix for adjacent elements.

Originally, Butler Matrices have typically employed 90° branch line couplers which inhibit performance. The wavelength dependent nature of these couplers forfeit size

frequency performance. The large sizes of these components have hindered the level of integration required for on chip implementation, making the Butler Matrices difficult for direct and compact on-chip integration.

In higher order Butler Matrices, the size becomes a critical issues. With each order the Butler Matrix more than doubles in area consumption. Therefore, for higher order networks, it is imperative to keep components small. However, to keep the size down, tradeoffs in performance are made throughout the network.

Butler Matrices define a general topology that uses scalable order to increase beam resolution at the cost of chip area. (A 2nd order matrix has 2^2 inputs and outputs while a 3rd order matrix has 2^3 .) As the order of the matrix increases the difficulty in design increases exponentially as well. In high order matrices, routing becomes non trivial due to numerous required crossovers and phase corrections. As the size increases the insertion loss is amplified by additional routing and passive loss of couplers. However, if the passive loss is small, the gain from the array can compensate with the increased directivity of the array. The example presented here is an 8×8 Butler Matrix based on a standard 65nm bulk CMOS that achieves low loss and ultra-compactness with proper phased-array beam forming.

Chapter 2

Theory

A Butler Matrix is a completely passive device that relies on couplers and phase shifters to divide and recombine signals propagating through the matrix to generate appropriate phase differences for beam forming. Butler Matrices can be categorized by their order, i.e. 2nd, 3rd, etc.. While a 1st order matrix is possible, calling it a Butler matrix would be a stretch, it is simply a coupler.

The analysis of a Butler Matrix begins with the coupler, Figure 5. It is known that a coupler has two outputs that are duplicates of the original signal with half the power and phase shifted with relation to the original and each other. The phase relation to the original signal has no bearing in the performance of the coupler or in the performance of Butler Matrices. However, the phase relationship between the *thru* and *coupled* signals is of the utmost importance and should be as close to 90° as possible. For example, a branch-line coupler has a theoretical phase shift of -90° from the *input* to *thru* port and -180° from the *input* to *coupled* port. The *coupled* port leads the *isolation* port by 90°.

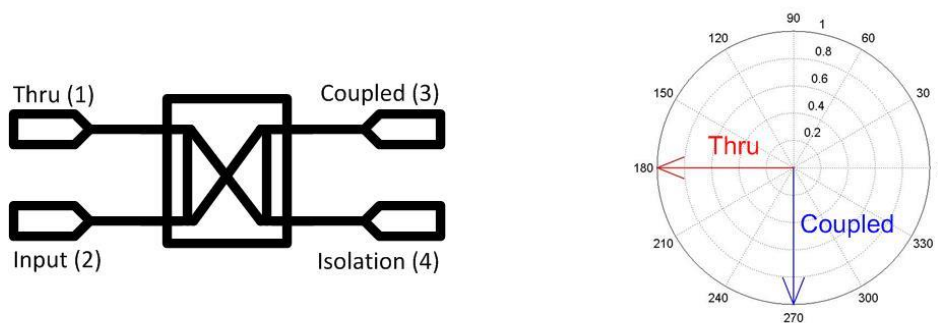


Figure 5. Coupler symbol and the branch line phase relations between the *Thru* and *Coupled* ports when excited from *Input*.

Using the phase difference created by the coupler it is possible to create a very simple array with a scanning angle off of broadside. Additionally, because the matrix is symmetrical if we excite the coupler from the isolation port, a similar phase relationship is established where the *coupled* port leads the *thru* port by 90° . If the phase difference between the input and output is not 90° , it becomes a problem when trying to create a proper beam-forming pattern in higher order matrices. For instance, if instead of the thru port leading by 90° it only leads by 60° then the phase difference between the two signals in the opposite direction around the unit circle is 300° instead of 270° . Beam forming issues caused by this error will be addressed later on.

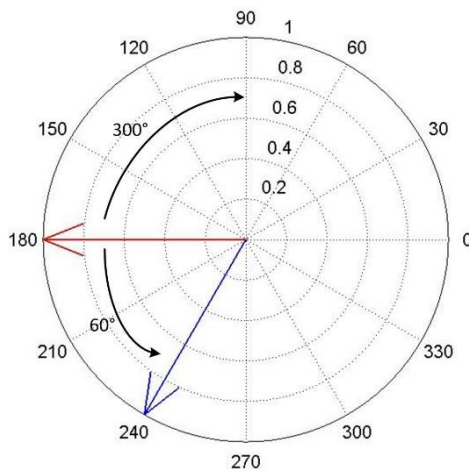


Figure 6. Degraded quadrature phase balance.

Because the network is passive, if both the *Input* and *Isolation* ports are driven simultaneously, the outputs will be a linear combination from excitation. The two ports chosen to excite the signal are isolated from each other when properly terminated. These statements can be summarized by an S-parameter characterization of the matrix,

$$\begin{bmatrix} V_1^- \\ V_2^- \\ V_3^- \\ V_4^- \end{bmatrix} = \begin{bmatrix} [Isolation \& Return Loss]_{2 \times 2} & [RX]_{2 \times 2} \\ [TX]_{2 \times 2} & [Isolation \& Return Loss]_{2 \times 2} \end{bmatrix} \begin{bmatrix} V_1^+ \\ V_2^+ \\ V_3^+ \\ V_4^+ \end{bmatrix}$$

$$= \frac{1}{\sqrt{2}} \begin{bmatrix} [0]_{2 \times 2} & e^{-j\frac{\pi}{2}} & e^{-j\pi} \\ e^{-j\frac{\pi}{2}} & e^{-j\pi} & [0]_{2 \times 2} \\ e^{-j\pi} & e^{-j\frac{\pi}{2}} & [0]_{2 \times 2} \end{bmatrix} \begin{bmatrix} V_1^+ \\ V_2^+ \\ V_3^+ \\ V_4^+ \end{bmatrix}$$

Because this coupler is passive its S-parameter matrix shows symmetry. This property is independent of order. The block matrices used in the S-parameters allow for easier characterization of higher order matrices. Although, not enough information is provided here the TX and RX block matrices are related by the transpose operation.

Continuing with a 2nd order Butler Matrix introduces new ideas that build on those introduced by the coupler. In a 2nd order matrix, each input signal is split divided two times implying that two rows of couplers are needed. However, if the Butler Matrix is left at that, the outputs will not be capable of exciting an array with a uniform phase tapers. Therefore, a phase shifter needs to be introduced to stagger the phase at the outputs.

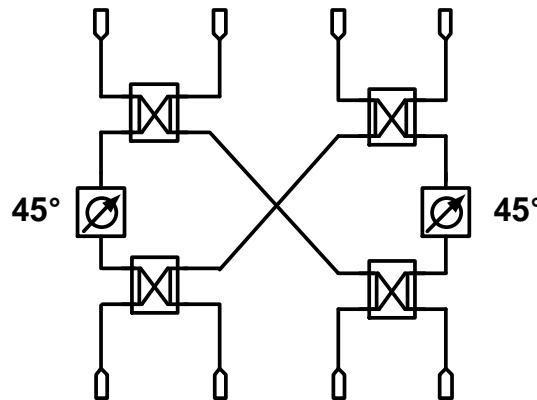


Figure 7. A 4x4 Butler Matrix topology excluding the antenna crossover.

In Figure 5 it was seen that there are two ways to describe the relation between the input and output of a coupler, 90° and 270° depending on the path around the unit circle. This difference can be bisected to create the phase differences 45° and 135° . Inserting a crossover at the outputs interweaves the outputs from the last couplers. This establishes a 45° phase difference at the antennas when excited from port 1, Figure 8. Carrying out a similar analysis, excitation from port two creates a 135° phase taper.

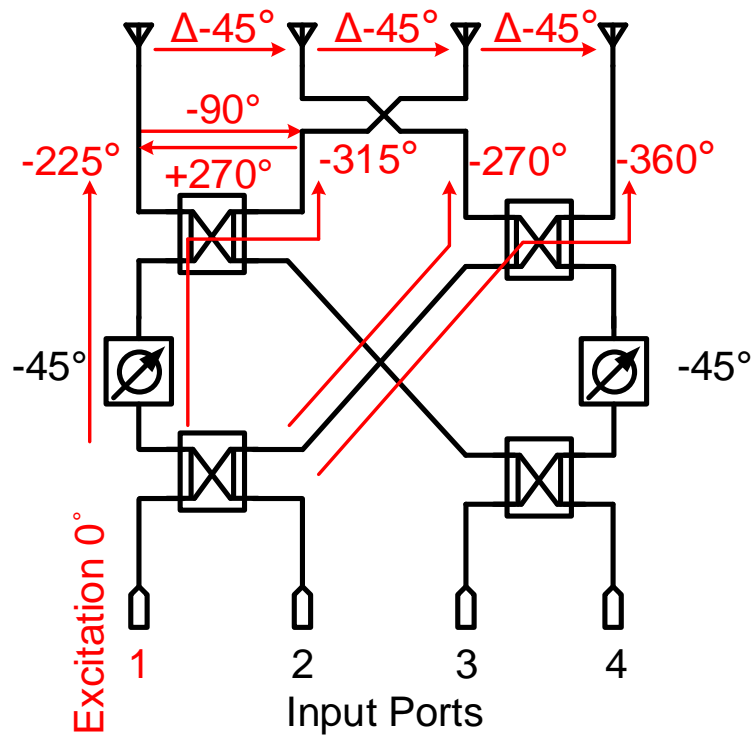


Figure 8. Phase relations when exciting the 4x4 Butler Matrix from port 1.

Staggering the output ports generated by quadrature couplers is common to any order Butler Matrix. A 3rd order Butler Matrix generates 8 beam patterns symmetric about broadside. By rotating 90° , 270° around the unit circle creates 4 beams. By making an additional rotation around the unit circle yields 450° and 630° for the additional beams.

This difference is subdivided into 4 equal phase differences resulting in 22.5° , 67.5° , 112.5° and 157.5° degrees phase differences, respectively.

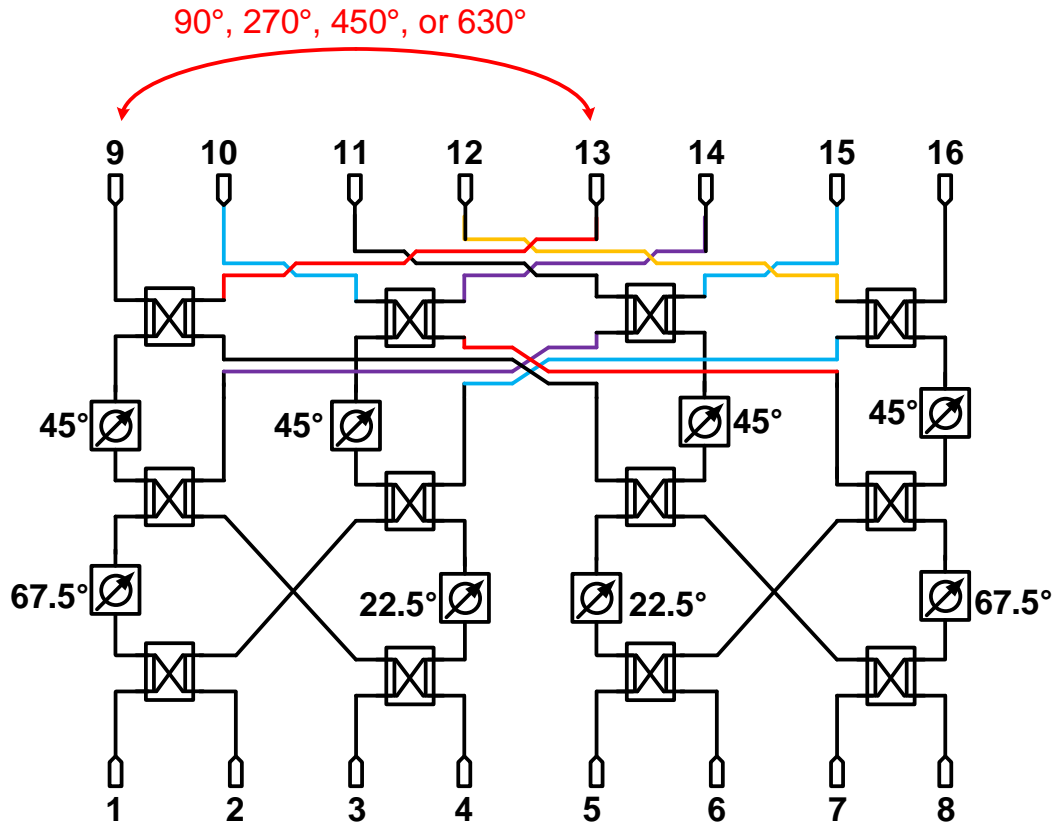


Figure 9. Modular coupler phase used to generate an 8x8 Butler Matrix's phase differences.

The design here presented here uses a transformer based swapped port coupler. The term swapped port makes the distinction of reversing the phase relationship between the *thru* and *coupled* ports. In a swapped port coupler instead of the *thru* port leading the *coupled* port by 90° , it lags the *coupled* port by 90° . This change does not dramatically alter the topology. It merely changes the location of phase shifters.

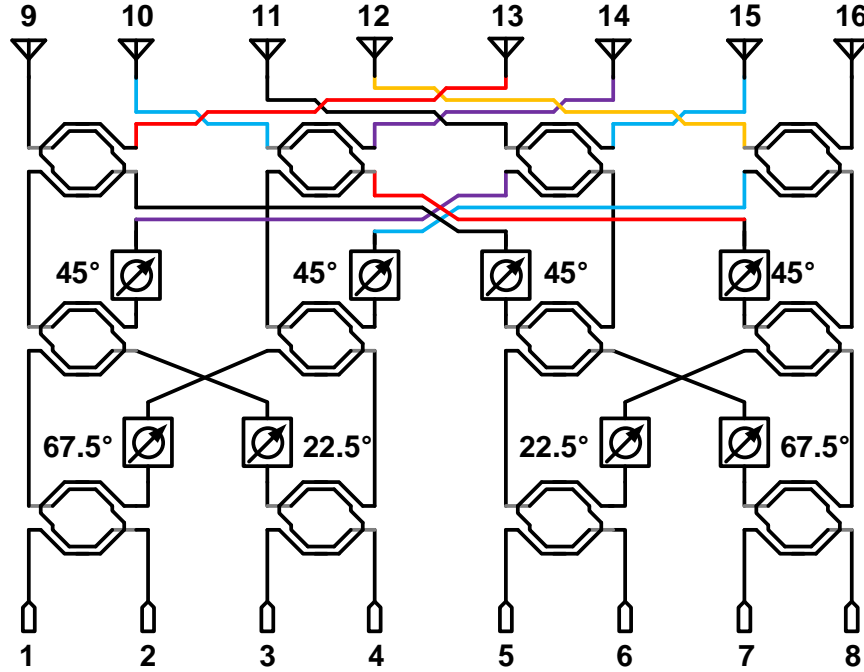


Figure 10. The 8x8 Butler Matrix using transformer-based couplers and port designations.

Assuming perfect matching and isolation between all stages we can construct an S-parameter matrix that describes the behavior of an 8x8 Butler Matrix by tracing the relative phase delays through the matrix. If the *input to thru* port is assigned a -90° phase shift and the *input to couple* port at 0° we can express the transmission matrix as,

$$[S]_{TX} = \begin{bmatrix} e^{-j\frac{12\pi}{8}} & e^{-j\frac{11\pi}{8}} & e^{-j\frac{10\pi}{8}} & e^{-j\frac{9\pi}{8}} & e^{-j\frac{8\pi}{8}} & e^{-j\frac{7\pi}{8}} & e^{-j\frac{6\pi}{8}} & e^{-j\frac{5\pi}{8}} \\ e^{-j\frac{8\pi}{8}} & e^{-j\frac{5\pi}{8}} & e^{-j\frac{6\pi}{8}} & e^{-j\frac{13\pi}{8}} & e^{-j\frac{4\pi}{8}} & e^{-j\frac{11\pi}{8}} & e^{-j\frac{2\pi}{8}} & e^{-j\frac{9\pi}{8}} \\ e^{-j\frac{9\pi}{8}} & e^{-j\frac{4\pi}{8}} & e^{-j\frac{15\pi}{8}} & e^{-j\frac{10\pi}{8}} & e^{-j\frac{5\pi}{8}} & e^{-j\frac{0\pi}{8}} & e^{-j\frac{11\pi}{8}} & e^{-j\frac{6\pi}{8}} \\ e^{-j\frac{5\pi}{8}} & e^{-j\frac{8\pi}{8}} & e^{-j\frac{11\pi}{8}} & e^{-j\frac{14\pi}{8}} & e^{-j\frac{1\pi}{8}} & e^{-j\frac{4\pi}{8}} & e^{-j\frac{7\pi}{8}} & e^{-j\frac{10\pi}{8}} \\ e^{-j\frac{10\pi}{8}} & e^{-j\frac{7\pi}{8}} & e^{-j\frac{4\pi}{8}} & e^{-j\frac{1\pi}{8}} & e^{-j\frac{14\pi}{8}} & e^{-j\frac{11\pi}{8}} & e^{-j\frac{8\pi}{8}} & e^{-j\frac{5\pi}{8}} \\ e^{-j\frac{6\pi}{8}} & e^{-j\frac{11\pi}{8}} & e^{-j\frac{0\pi}{8}} & e^{-j\frac{5\pi}{8}} & e^{-j\frac{10\pi}{8}} & e^{-j\frac{15\pi}{8}} & e^{-j\frac{4\pi}{8}} & e^{-j\frac{9\pi}{8}} \\ e^{-j\frac{9\pi}{8}} & e^{-j\frac{2\pi}{8}} & e^{-j\frac{11\pi}{8}} & e^{-j\frac{4\pi}{8}} & e^{-j\frac{13\pi}{8}} & e^{-j\frac{6\pi}{8}} & e^{-j\frac{5\pi}{8}} & e^{-j\frac{8\pi}{8}} \\ e^{-j\frac{5\pi}{8}} & e^{-j\frac{6\pi}{8}} & e^{-j\frac{7\pi}{8}} & e^{-j\frac{8\pi}{8}} & e^{-j\frac{9\pi}{8}} & e^{-j\frac{10\pi}{8}} & e^{-j\frac{11\pi}{8}} & e^{-j\frac{12\pi}{8}} \end{bmatrix}$$

Where,

$$\begin{aligned}
 \begin{bmatrix} V^- \end{bmatrix}_{16 \times 1} &= [S]_{16 \times 16} \begin{bmatrix} V^+ \end{bmatrix}_{16 \times 1} \\
 &= \begin{bmatrix} [0]_{8 \times 8} & [S]_{RX} \\ [S]_{TX} & [0]_{8 \times 8} \end{bmatrix} \begin{bmatrix} V_1^+ \\ \vdots \\ V_{16}^+ \end{bmatrix} \\
 &= \begin{bmatrix} [0]_{8 \times 8} & [S]_{TX}' \\ [S]_{TX} & [0]_{8 \times 8} \end{bmatrix} \begin{bmatrix} V_1^+ \\ \vdots \\ V_{16}^+ \end{bmatrix}
 \end{aligned}$$

establishes the relationship between the incident wave and transmitted waves. Using this matrix we can create an electrically synthesized beam pattern showing the received power at each port based on the phase difference received from the antennas.

$$\begin{aligned}
 \begin{bmatrix} V_1^- \\ \vdots \\ V_8^- \end{bmatrix}_{8 \times 1} &= [S]_{RX} \begin{bmatrix} V_9^+ \\ \vdots \\ V_{16}^+ \end{bmatrix}_{8 \times 1} \\
 &= [S]_{RX} \begin{bmatrix} 0 \\ \theta \\ \vdots \\ 7 \times \theta \end{bmatrix}_{8 \times 1}
 \end{aligned}$$

Note in this equation, ports 9-16 represent the ports feeding the antenna array as established in Figure 10. The electrically synthesized shows both signal combination and cancellation where each input port demonstrates a main lobe for a unique phase difference, Figure 11.

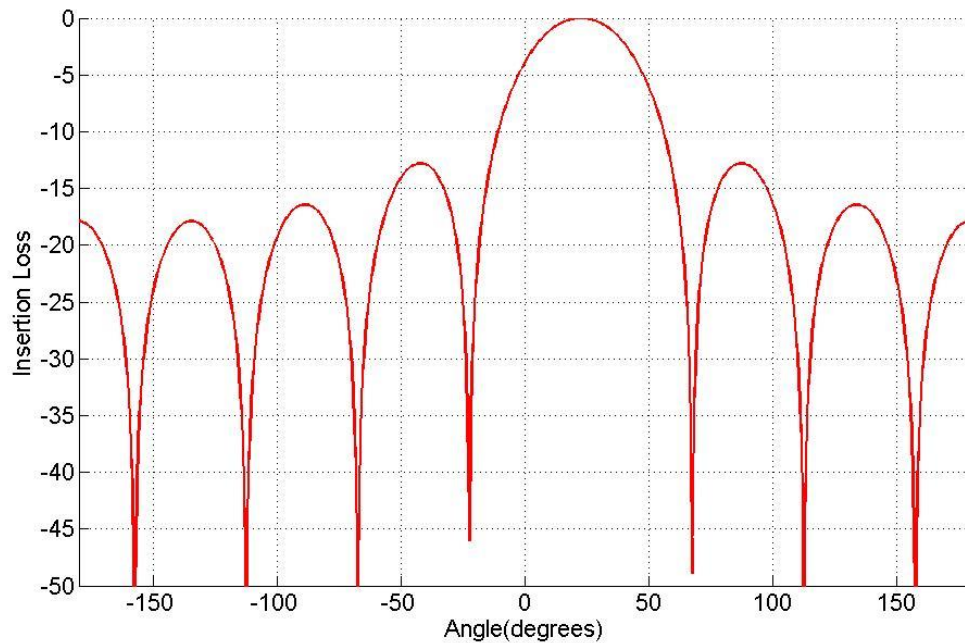


Figure 11. Ideal electrically synthesized beam IR (port 1) of the swapped port 8x8 Butler Matrix.

The response generated in Figure 11 analogous to the array factor pattern of a linear array. Here, the response of port 1 is plotted against a swept phase difference. The peak corresponds to a phase difference of 22.5° . This phase difference corresponds to a physical angle determined by the spacing of the elements in a linear array.

A measure of performance used here is the peak-to-null (PNR). This is an overall metric of performance that accounts for phase and amplitude performance as well as loss of the system. With a Butler Matrix the PNR of the system will be infinite as out-of-band signals cancel perfectly. As errors in phase or amplitude develop, the Butler Matrix no longer exhibits perfect cancellation and the nulls begin to increase and peaks decrease in magnitude and change measured peak phase difference, Figure 12.

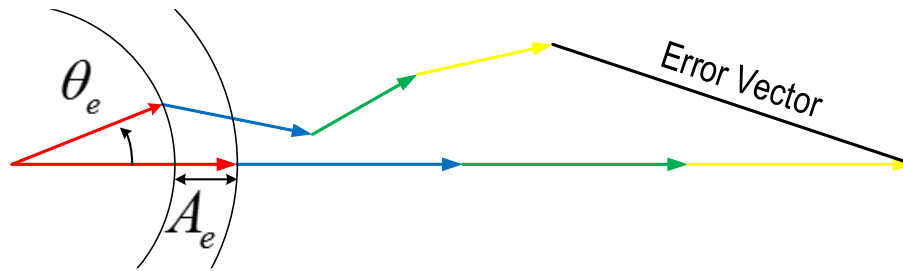


Figure 12. Amplitude and phase error are responsible for an error vector and degrade PNR performance.

Transformer Based Quadrature Coupler

One main hindrance of implementing Butler Matrices on Silicon has been the bulky size of quadrature generation from passive components such as the branch line coupler. The branch line coupler realizes 90° phase shift from the physical length of the lines. Even and odd mode analysis of the structure shows that when the electrical length of the branches is a quarter wavelength the input signal is split equally between the thru and coupled ports. As the frequency of operation moves off from the frequency the coupler was intended to operate at, the performance of the coupler quickly degrades. Instead of using distributed couplers the work here leverages a transformer based coupler.

In order to assess performance of the coupler we need to establish the parameters of the coupler that are of importance. These are:

- Port Matching
- Adjacent Port Isolation
- Passive Loss
- Amplitude Balance

- Phase Balance

Port matching aids to keep the matrix unilateral, maintain phase balance, and amplitude balance. Without matching the devices cannot be simply cascaded as needed in the design. Because of the complexity of the design and layout, it is necessary to design cascadable blocks and combine them as the design progresses instead of designing the Butler Matrix as a whole, in addition loading the coupler with an unmatched load can adversely affect the phase and amplitude balance of the coupler.

Isolation prevents signals from one port leaking through to the adjacent ports. If two adjacent signals are not isolated signals may be masked by this leaked power. During operation at most two ports will be receiving or excited simultaneously. In this case the value of isolation is apparent and necessary to maintain the individual signal integrity. In single port excitation if power is leaked to an adjacent port, this power is absorbed by the input termination. In the case of receiving, this power is reflected back out. Depending on the application, this leaked power could be problematic.

As each coupler splits a signals into two equal component. The components at the *thru* and *couple* ports will, without any additional loss, attenuate by 3dB. Any additional loss is termed passive loss and can come from a variety of reasons, e.g. finite conductivity and substrate losses. These signals need to be balanced so that during reconstruction out of beam signals cancel. With unequally balanced signals there is residue which degrades matrix performance. From the perspective of transmission, unequal amplitude balance can increase side lobe levels.

The layout of the coupler which will be shown later lies above a ground cutout so there is no barrier between the coupler and the lossy silicon substrate. Patterning a ground plane can reduce loss.

To demonstrate the effects of phase imbalance consider the 4x4 Butler Matrix case present in Figure 13. Here, instead of the coupler generating quadrature signals, the outputs are only separated by 60° in phase. In the case of *Excitation 2*, the phase shifter is change from 45° to 30° in order to compensate for the error in quadrature generation. The output shows that, for this excitation, the array maintains a uniform phase difference between elements. However, *Excitation 1* does not exhibit this uniform phase difference. Only one path can be compensated by adjusting the phase shifter. Therefore, a 90° phase shift must be generated by the coupler.

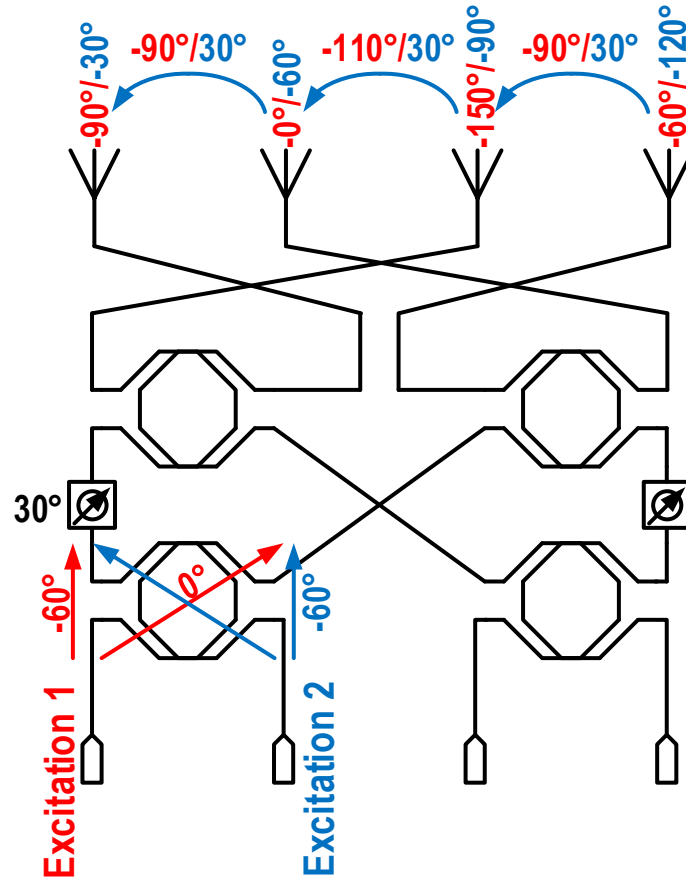


Figure 13. Partial compensation of coupler phase error with phase shifter.

In addition to the large size of the branch line coupler, the bandwidth of the coupler can also be improved upon. A direct dependence of the bandwidth to the physical length limits the achievable bandwidth using a basic coupler. There are techniques available to improve the bandwidth of the basic branch line coupler but these do not address the size of the coupler.

The transformer based quadrature generation method chosen here has previously been presented and analyzed [13] and used with good results in [14]. The transformer is two intertwined inductors that use mutual inductance and capacitive coupling to split inputs into quadrature signals with equal amplitude and 90° phase shift at resonance. By avoiding wavelength based transmission lines, the quadrature generation is realized in a

tighter area than its bulky counterparts. While the phase balance is extremely broadband, the amplitude balancing, however, is not. The transformer in essence provides a high pass and low pass path from the *input* port to the *thru* and *couple* ports, respectively, creating a single frequency crossover.

The comparison that follows measures how the transformer based coupler stacks up against the standard branch line coupler. While the branch line coupler has comparable response in terms of the amplitude balance the phase imbalance becomes severely exaggerated away from center frequency. A Lange coupler is another quadrature hybrid that exhibits superior wideband phase performance with respect to either the branch line or transformer based coupler. However, the tradeoff of the microstrip Lange coupler is the size. The fingers of the basic Lange coupler are 90° in length. Even at high frequency this is considerable, $\sim 670\mu\text{m}$ at 60 GHz with an effective permittivity of ~ 3.5 (based on a rough average of the permittivity of the process). The size is prohibitive from implementing the Lange coupler on chip but is worth mentioning for the application due to its wideband phase performance. Ultimately, the transformer based coupler is used in the example due to its extremely small size. The outside diameter of the coupler presented has an outer diameter of $86\mu\text{m}$ with a $5\mu\text{m}$ trace width and $4\mu\text{m}$ trace spacing.

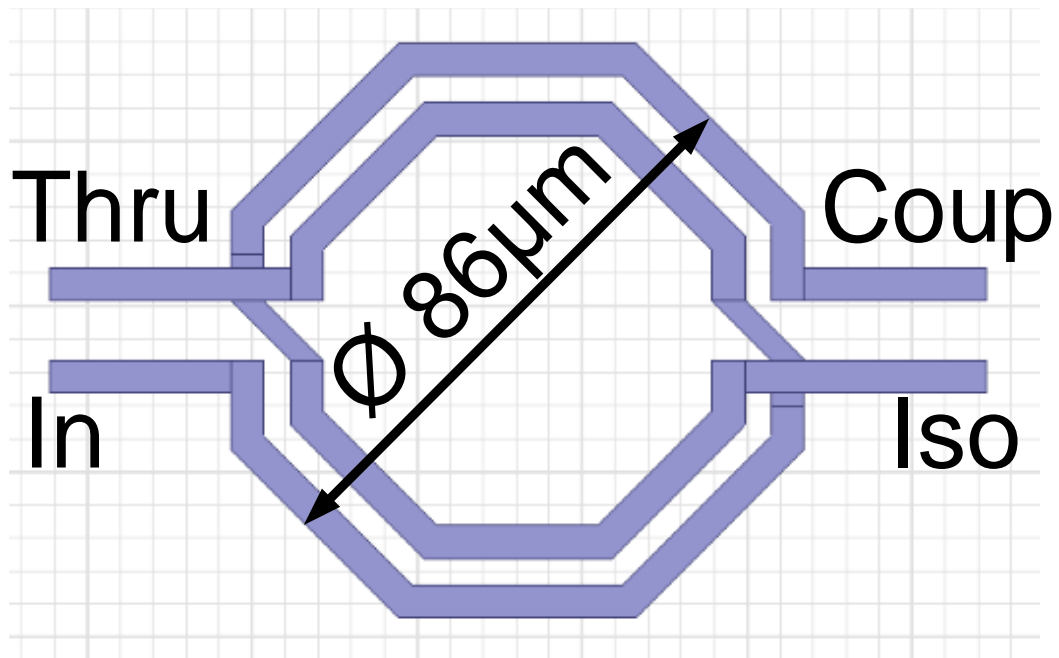


Figure 14. EM structure of the transformer based coupler.

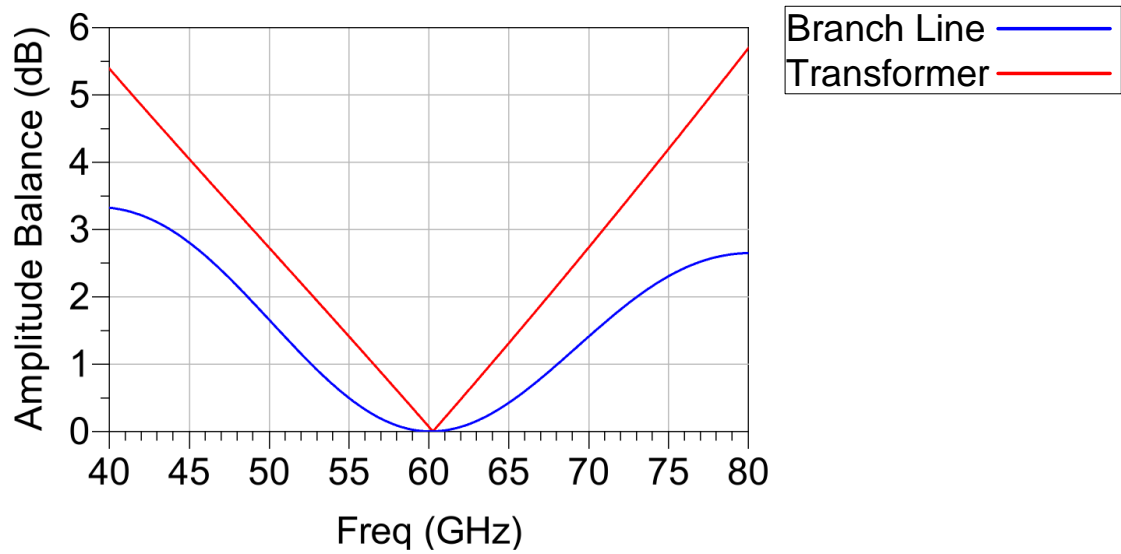


Figure 15. Amplitude balance comparison of the branch line and transformer based coupler.

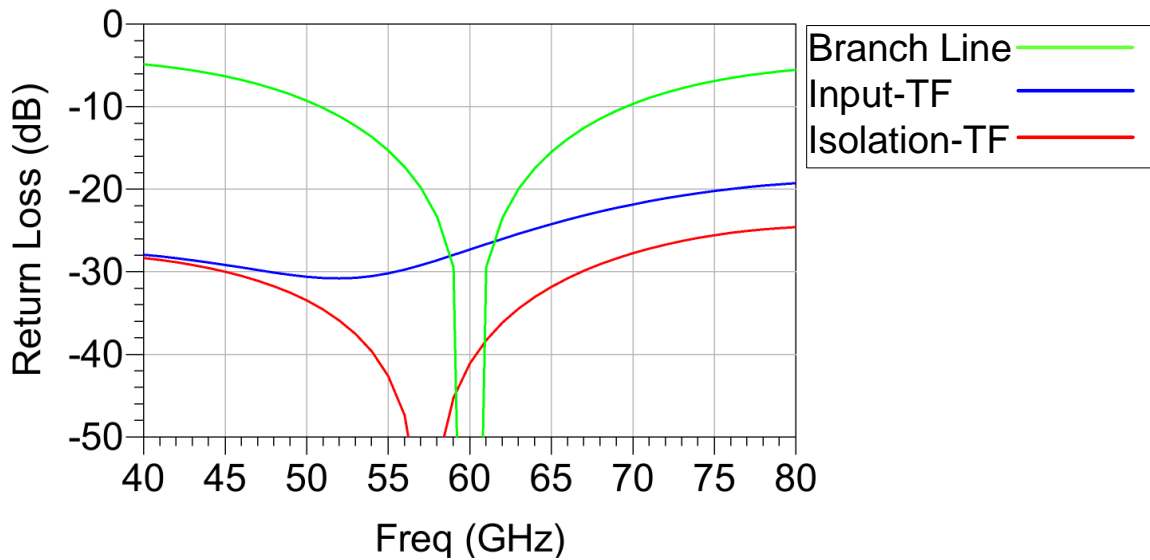


Figure 16. Input matching comparison of the branch line and transformer based coupler.

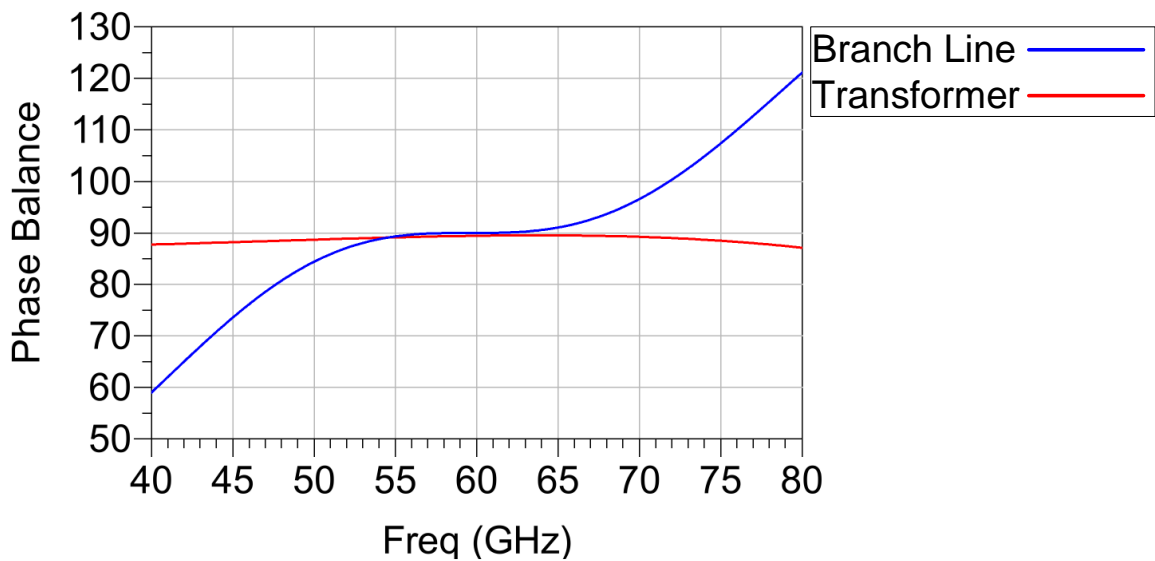


Figure 17. Phase balance comparison of branch line and transformer based coupler.

Phase Shifter

To create the necessary phase differences between the antenna ports, beam forming networks require numerous phase shifters throughout the structure. These phase shifters offset the outputs generated by the couplers. In a 4x4 Butler matrix, a 45° staggers the outputs to create a uniform 45° phase difference at the antenna ports. In an 8x8 Butler

Matrix this minimum phase difference is defined to be 22.5° so we see 22.5° , 45° and 67.5° phase shifters to stagger the outputs.

In passive structures these delays can be implemented as meander lines. The pitfall of the meander line is the size required to achieve the desired phase shift. The delay is simply the velocity of propagation through the medium divided by the wavelength. Thus, the phase of the meander line is proportional the frequency of operation.

$$\theta = \frac{l}{\lambda_e} \times 360^\circ$$

$$= \frac{l \times f}{c} \times 360^\circ$$

Where l denotes physical length and λ_e represents the effective wavelength in the medium.

When the phase delay becomes large the size of the meander line required to implement it becomes disagreeable. To reduce the area consumed, the designer can implement these shifts using C-L-C π -networks. The C-L-C π -networks allows for input and output matching with a phase delay between input and output ports based on the component values.

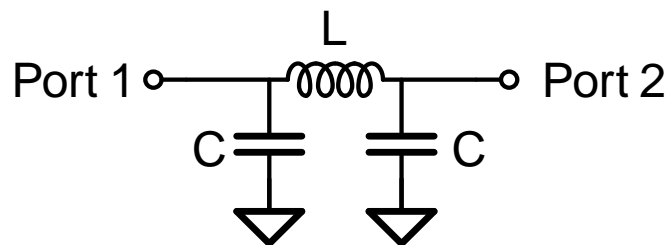


Figure 18. C-L-C π -network circuit.

The equations governing the phase delay, matching characteristics are as follows.

$$C = \frac{\tan\left(\frac{\theta}{2}\right)}{\omega Z_0}$$

$$L = \frac{Z_0 \sin(\theta)}{\omega}$$

From these equations, it is immediately noticed that there exists an asymptotic limit as 180° is approached. In general, it should be avoided trying to design a phase shift that lies close to 180° . Designing close to 180° brings a resonant point near the design frequency which will yield a nonlinear phase response around the frequency of operation. In addition to degraded phase response the inputs will not be matched near the resonant point. In the application of the Butler Matrix, the phase shift required by the matrix will never exceed 90° .

The tradeoff in design with the meander line comes from the practical side. Why use a lumped element phase shifter instead of a delay line or when should a meander line be used? The tradeoff is size and loss. The delay line will grow in length proportionally to the size of the delay required. By using a lumped element phase shifter though, as the diameter of the inductor grows there reaches a point where the number of turns can be increased. By increasing the number of turns in the inductor, the growth rate is retarded making it a more area efficient choice for large delays.

The decision flow in this work used C-L-C π -networks when the delay met a minimum requirement. This minimum value was determined by the DRC of the process.

Because of trace spacing, there exists a minimum loop size for the inductor. For small phase delays, meander lines were selected. As the delay continued to increase phase shifters were implemented using π -networks. The only phase delay in the design meriting a π -network was the 67.5° phase delay path.

An additional tradeoff in the design is the finite Q of the shifter. Here the low Q of the capacitors contributes to the loss of the phase shifter and can add a significant amount of loss depending of the frequency of the design.

Antenna Array

The actual beam forming is a result from arraying the antenna elements. For a Butler Matrix, the antenna array is has a linear uniform spacing and uniform amplitude excitation when excited from a single port. Some of the performance specifications for an array are the peak gain, side lobe level and scan angle.

The performance of the antenna array is described by the array factor. The array factor can be calculated through the vector addition of each independent plane wave generated by each antenna. This is an ideal calculation that neglects the physical effects such as coupling between elements and spurious radiation from the feed network. The array factor of a uniform linear array can be expressed as

$$AF_N = \left(\frac{\sin \frac{N\Psi}{2}}{\sin \frac{\Psi}{2}} \right)$$

where

$$\Psi = kd \cos \theta + \beta .$$

In the above equation, k represents the wavenumber of free space, d the physical spacing between elements and, β the phase difference between elements. The array factor expressed here is valid for scanned arrays as well and we can estimate the radiation pattern for the Butler Matrix using this equation and the theoretical phase differences generated by the Butler Matrix. For an isotropic antenna the array factor for half space is shown in Figure 19. This array factor represents the normalized radiation pattern for an element spacing of $\lambda/2$.

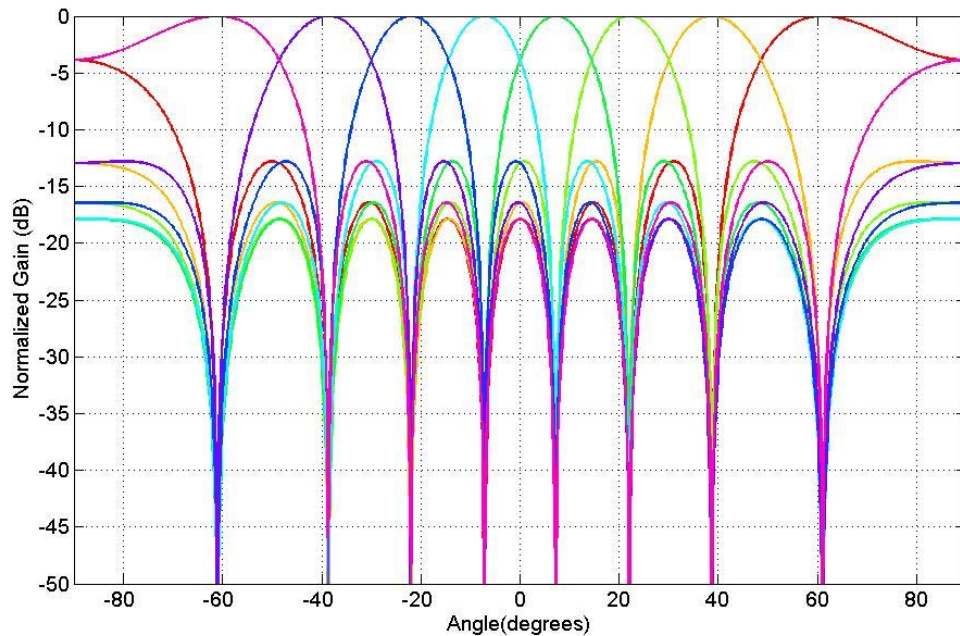


Figure 19. Array factor for an 8 element linear uniform amplitude and uniform spaced array.

Each of the eight beams formed correspond to a specific port excitation to the Butler Matrix. Each input to the matrix corresponds to a unique value of β . This value is translated to a scan angle based on the design of the antenna array.

One major limitation of the uniform linear array is the side lobe level. Above, with a spacing of $\lambda/4$ the side lobes can be calculated to be -13.46dB relative to the main beam. To overcome the inherent limitation, the superposition of two signals can be used to create a cosine taper in signal amplitude. If a signal is applied to 4R with phase delay of 180° and 3R with a phase delay of 22.5° the Butler Matrix linearly combines these signals to create pattern resembling a cosine taper. A comparison of an idea Butler Matrix with 4R and 3R excitation is compared to an ideal cosine distribution in Figure 20.

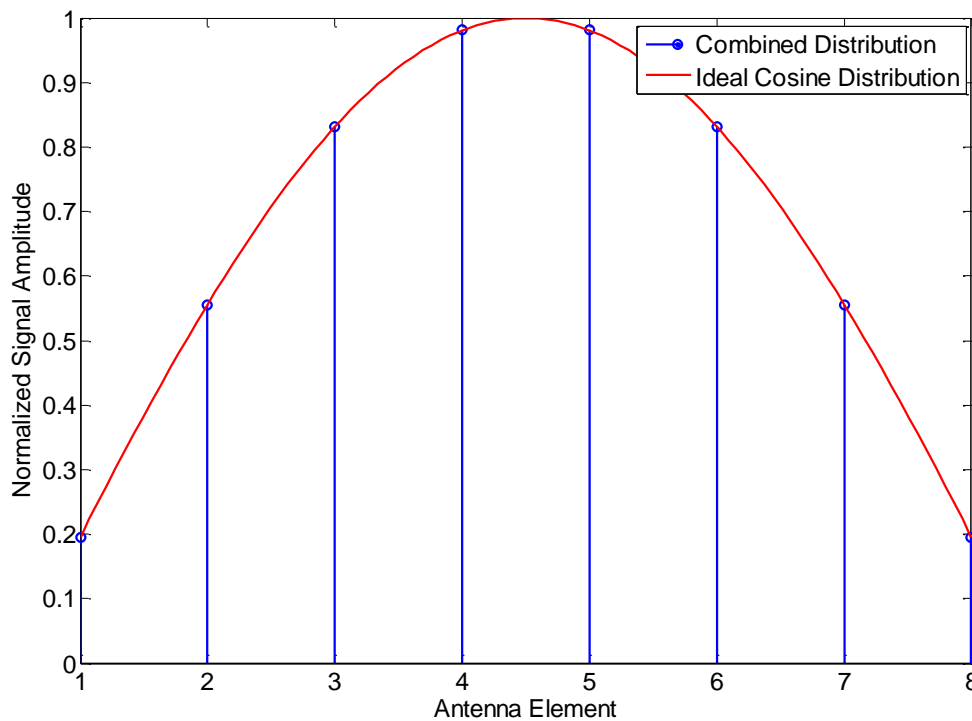


Figure 20. Signal distribution of combined excitations and ideal cosine distribution of antenna elements.

By using a cosine amplitude distribution compared to a uniform distribution the side lobes of the array are reduced. This can improve the theoretical side lobe level to -23dB.

Chapter 3

Butler Matrix Design

Technology

The design for this example Butler Matrix is based in a standard 65nm bulk CMOS process. The metal layer stackup is shown in Figure 21. The process offered a top aluminum and thick metal layer for signals as well as a semi global and intermediate metal layers. The aluminum and thick metal layers made up a bulk of the design here as they were the thickest metals available to reduce the loss of the matrix. The global layer was chosen to be used the ground layer.

The process used was not amicable to the implementation of the Butler matrix due to the metal layer fill, physical dimensions, and DRC requirements. The process used had two a top aluminum layer followed farther down by a thick copper layer. Because of the copper metal layer's proximity to the lower metal layers, this layer could not be matched to 50Ω without violating the minimum trace width. As a result, a top aluminum layer was used. This resulted in an exchange of proper matching for higher loss.

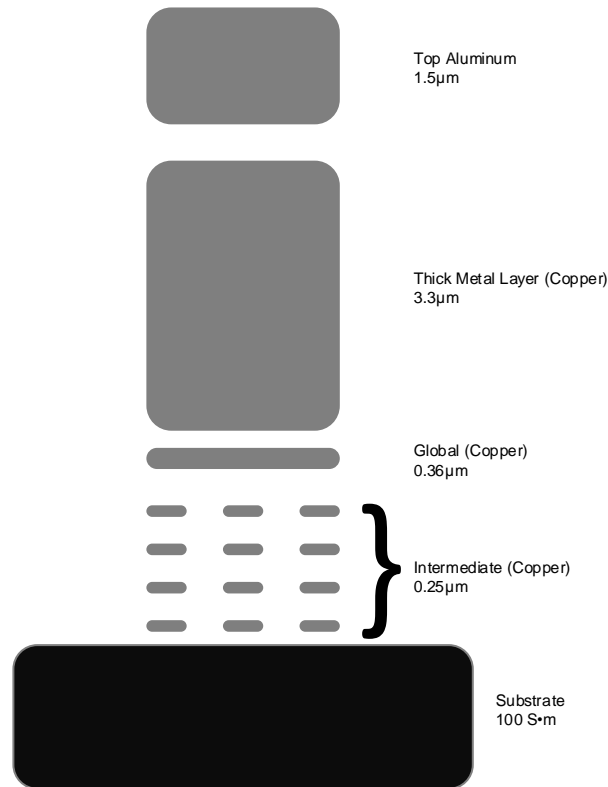


Figure 21. Metal layer stackup for the 65nm Bulk CMOS process.

Validation

The first part of the design process begins with verifying an EM model stackup. A replica stackup was created in HFSS® according to the process stackup. Before starting any design work, this stackup needs to be compared to models provided. In this design, validation comprised of matching dielectrics in the models to the testing data provided to the foundry. Tuning simulation data to test data helps ensure simulated models will behave in a similar fashion to the fabricated device.

The stackup verification was performed using a series micro strip transmission lines. For a given width, length and ground reference, the foundry model transmission line has a specific impedance and phase delay at a given frequency. These foundry models were developed and tested to 40GHz but it is assumed that due to the passive nature the

simulated behavior can be extrapolated to 60GHz and above if the performance is matched at the lower frequencies.

To start, a transmission line model from Cadence® was exported from layout to a GDSII format file and imported to HFSS®, Figure 22. This model was then simulated in HFSS® to generate the S-parameters for the structure. Initially these parameters, did not match in phase or matching performance. These S-parameters were converted to Z-parameters to calculate the characteristic impedance of the transmission line.

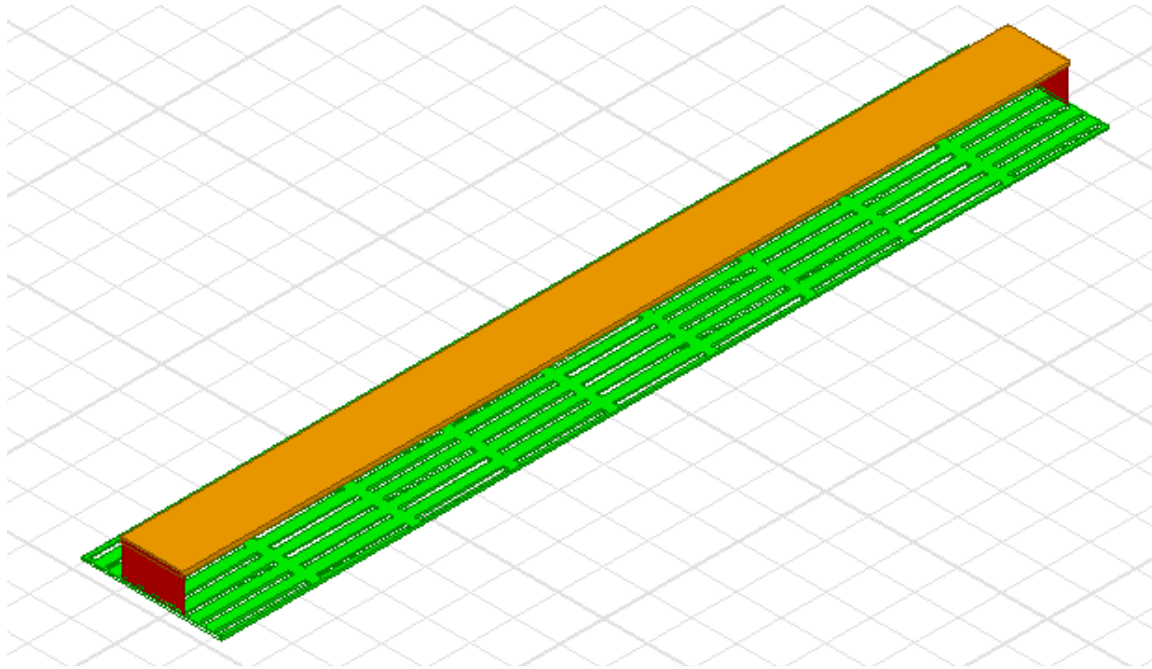


Figure 22. Imported GDSII stream file from Cadence® used to validate stackup.

From transmission line theory is known that the input impedance of short circuited and open circuited transmission line can be expressed as

$$\begin{aligned} Z_{in} &= jZ_0 \tan(\beta l) \\ Z_{in} &= -jZ_0 \cot(\beta l) \end{aligned}$$

respectively.

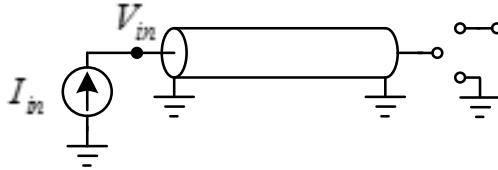


Figure 23. Two load conditions to determine transmission line characteristic impedance.

There are now two equations and two unknowns that can be solved for. One is the phase shift, βl , and the second is the characteristic impedance of the line, Z_0 , both of which need to match the model data provided. In the design of the transmission line many of the variables that control the characteristic impedance of the line are fixed i.e. height, width, etc. To vary the characteristic impedance we look to the very basic equation derived from transmission line theory for an ideal lossless line.

$$Z_0 = \sqrt{\frac{L}{C}}$$

Since $C \propto \epsilon_r$, by changing the relative permittivity we can change the characteristic impedance and the phase delay of the transmission to match what is predicted by the models provided. By adjusting the relative permittivity of surrounding layers, the phase was matched within a degrees and return loss within 1dB.

This method should be performed through the various dielectrics stacks present in the design. Here the global layer served as the ground plane while the thick metal and aluminum layers were used to create the beam forming network core. The transmission lines are verified for each case; the thick metal layer to the ground plane, and the aluminum layer to the ground plane. Once this is completed we can begin laying out the network.

EM Model Layout

Care is given to the layout of the network as one change can have a vast impact on the network as a whole. For instance if the coupler size changes in the design, this will change routing lines between elements which can cause a change in the phase shift of these lines and this phase shift will invalidate the current routing.

Therefore, the first part of the design process is creating a model for the transformer based coupler. This will be a repeating component. It determines the spacing for delay lines and the general structure of the matrix. All other components will be routed around them.

All the signals are routed on the top aluminum layer using microstrip lines to keep the fields contained above the silicon substrate. By separating the transmission lines from the substrate loss is reduced because no fields enter the substrate.

After the model for the transformer is finished, routing between couplers needs to be phase matched to the smallest relative phase delay. Referring to Figure 24, the path in red is recognizable as the shortest length trace connecting the first and second row of couplers. This path has a 0° phase shift relative to the rest of the paths, the paths in yellow and red must attain a phase delays of 22.5° and 67.5° relative to the shortest path, respectively. A portion of the 22.5° phase shift is made of by the horizontal component that the trace has to traverse, the remainder of this phase shift is achieved using a meander line. The 67.5° phase shift needs an additional 45° relative to the 22.5° path. The phase shift of the meander line and the additional 45° phase shift is compensated through the use of the C-L-C π -network. A visual comparison of the C-L-C π -network and

meander line for the two paths shows very similar area even though the phase shifter achieves more close to 3 times the phase delay.

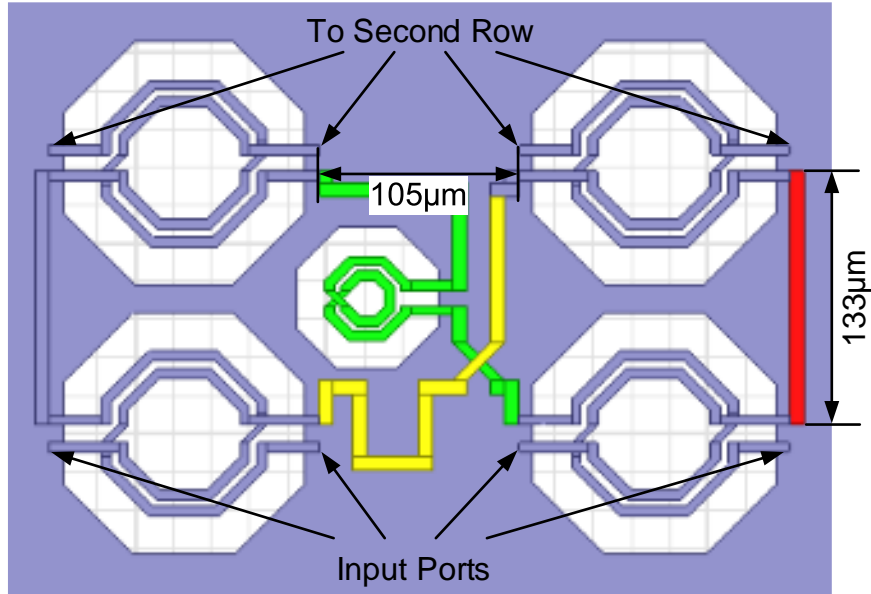


Figure 24. First phase matching stage showing minimum phase path (red), 22.5° path (yellow) and 67.5° path (green).

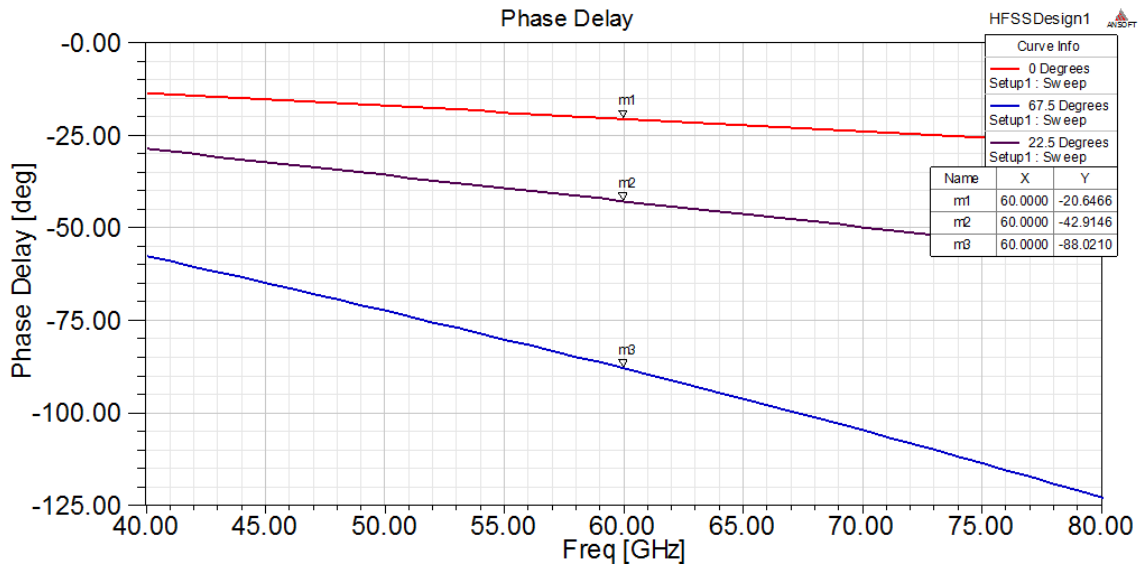


Figure 25. Phase matching quality of the different paths.

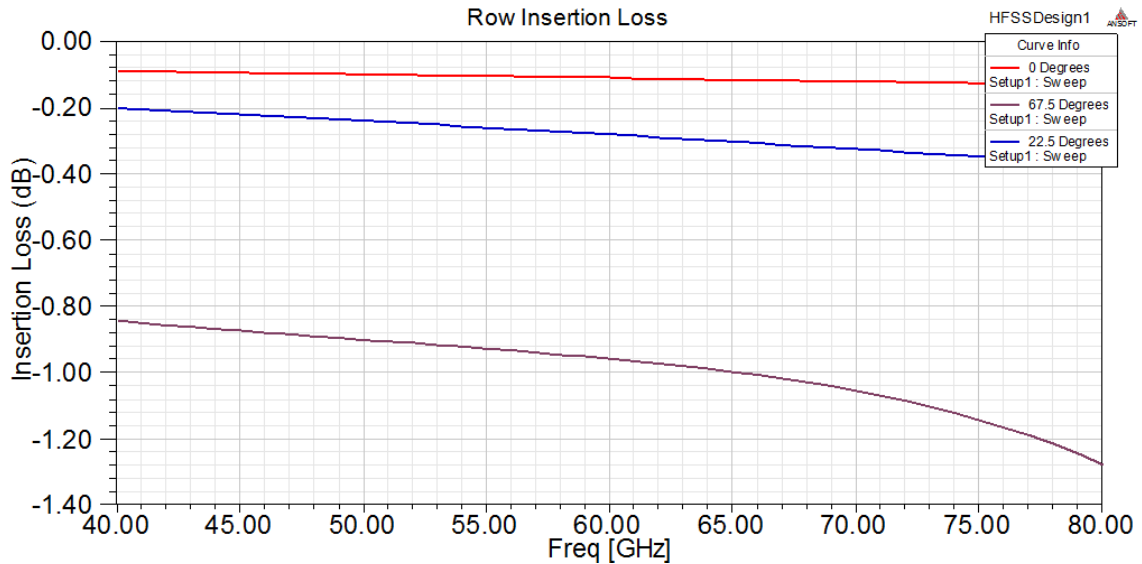


Figure 26. Loss comparison of different paths.

Figure 26 shows that the loss of the π -network is an additional tradeoff in realizing a 67.5° phase delay. The insertion loss of the 22.5° path shows a loss of $\sim 0.3\text{dB}$, 0.19dB more than the shortest path, while the path of the 67.5° phase delay shows a loss of $\sim 0.9\text{dB}$, 0.79dB more than the shortest path. A comparison between the phase shifting methods is shown in Table 1. The measurement of the π -network includes the ground ring spacing in the area measurement. The difference in the insertion loss of each path creates an undesirable effect reducing the peak to null ratio of the matrix.

Table 1. Phase shifter comparison at 60 GHz.

Phase Delay Method	Relative Length	Phase Delay	Loss	Loss/ $^\circ$	Area
Straight Line	0°	20.65°	0.11dB	$5.33\text{m dB}/^\circ$	N/A
Meander Line	22.5°	42.91°	0.28dB	$6.53\text{m dB}/^\circ$	0.0019mm^2
π -network	67.5	88.02°	0.96dB	$10.91\text{m dB}/^\circ$	0.0043mm^2

The Butler Matrix is symmetrical so the set of 4 couplers in Figure 24 is mirrored before the final row of couplers is added on. The spacing between this bottom set of couplers is spaced to reduce coupling between microstrip lines. With these two blocks in

place, the traces between the second and third row of couplers can be routed. The lines shown in red require a phase delay of 45° relative to the green traces. A majority of this phase delay is acquired during the routing a trace from its origin to its destination. The small amount of remaining delay is corrected with meander lines.

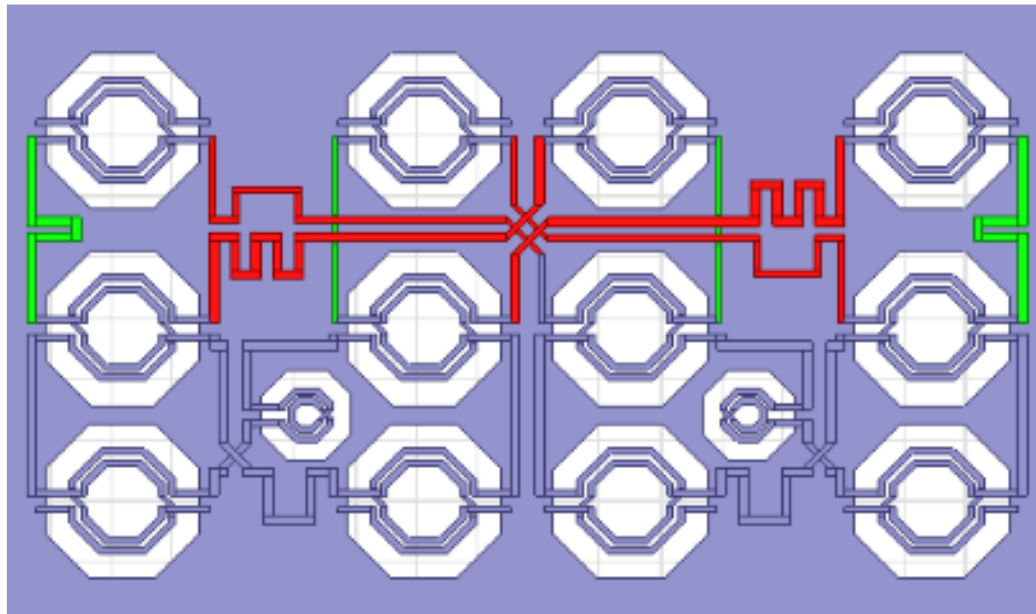


Figure 27. Second stage phase matching stage with 0° paths (green) and 45° paths.

To make the connections between the rows, crossovers have to be included. In these crossovers the routing drops down to the thick metal layer. However, this layer cannot be matched to the 50Ω characteristic impedance the rest of the matrix uses. The mismatch caused by the decreased width is compensated by adjusting the width of the remainder of the line. While this provides matching at the design frequency, it is not a broadband solution. The equivalent structure for this circuit is as shown in Figure 28. This structure is designed so that looking into either side is matched to 50Ω and is similar to a stepped impedance transmission line filter.

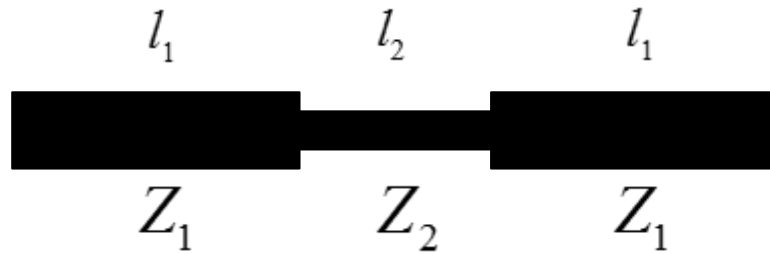


Figure 28. Stepped impedance filter as a crossover.

Measurements and phase relations of the second row are established in the same manner as they were established in the design between the first two rows of couplers. The coupling between all paths is less than 20dB. It is important to keep the coupling low as it can degrade the phase and amplitude performance of the matrix.

At this stage the core structure of the matrix is complete, the size of this structure measures $0.82 \times 0.39 \text{mm}^2$ in size. A single branch line coupler in a comparable substrate would have an area of roughly $0.625 \times 0.625 \text{mm}^2$. In comparison, this core area of this Butler Matrix is a factor of 1.1 times less than a single branch line coupler.

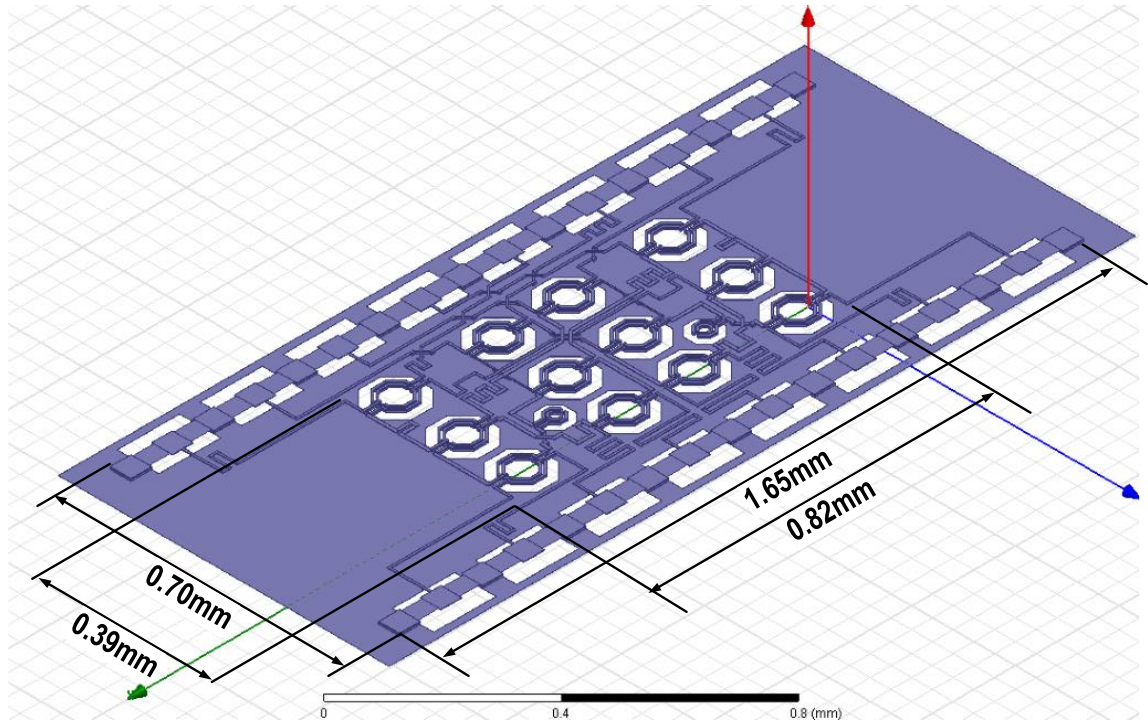


Figure 29. HFSS® EM final metal layout structure and core dimensions.

Both the input and output to the network have meander lines to phase match all lines attached to the core of the matrix. Additionally, the output of the matrix incorporates the antenna crossovers. Including the antenna crossovers on chip eases the off chip routing. The outputs use a 100 μ m pitch GSG spacing with shared ground pads. The ground underneath the pads is cut out to reduce capacitance for impedance matching.

Design for Test

To complete the practical design, some consideration must be given to the method of testing. The problem of testing arises from the available equipment and required operating conditions of the Butler Matrix. In the design of the coupler it was assumed all ports are terminated to the characteristic impedance. Termination to unmatched loads adversely affects all aspects coupler performance. Using wafer probes it is possible to probe only up to 4 ports at the same time using GSGSG probes in combination with a 4

port network analyzer and only two ports using single GSG probes. While these probes provide the termination for ports they are connected to, the network needs an additional method to terminate the remaining ports.

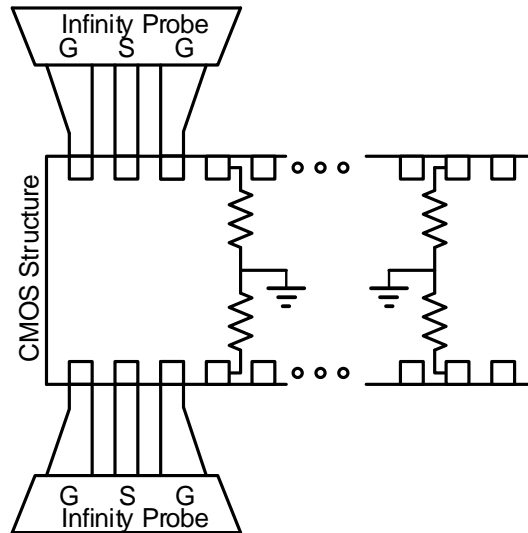


Figure 30. Testing setup showing the termination limitation of probes.

To solve this problem a switch with an on resistance of roughly 50Ω is used. In the off position, these switches need to have an impedance high enough not to degrade the matching of the circuit. Using extracted circuit parameters from Cadence® a rough equivalent parallel RC circuit, Figure 31, was added close to the pads to terminate the ports when not connected to the probes, Figure 32. The termination transistor is placed as close to the edge of the ground plane cut out as possible. The transistor was placed at the edge of the ground plane next to the pad cutout. This was done to reduce any inductance that might be added by routing a trace under the bond pad. By placing the transistor at the edge of the cutout leaves an open circuited transmission line.

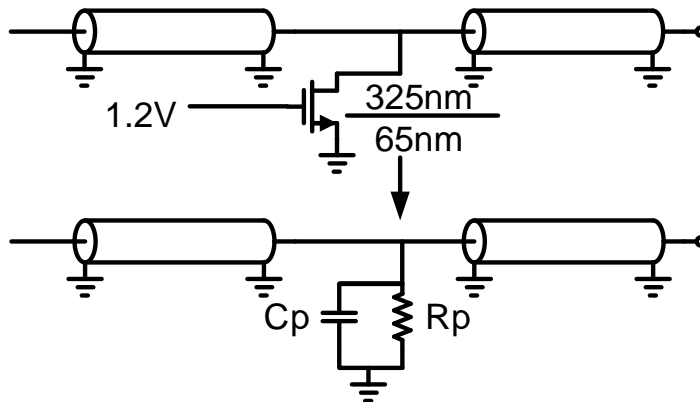


Figure 31. Equivalent model for the termination transistors.

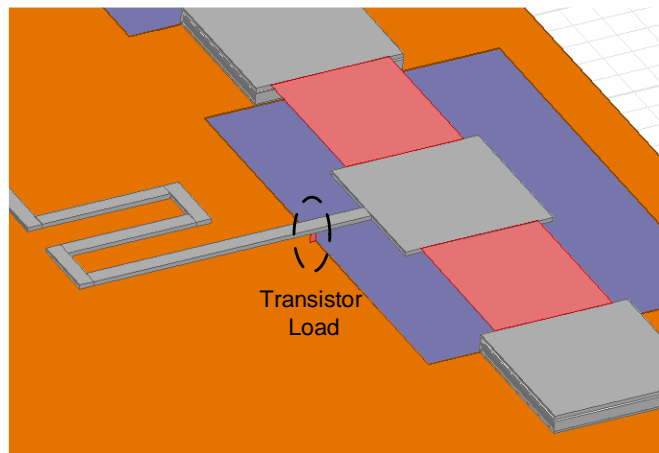


Figure 32. Equivalent termination transistor model at the edge of the ground plane.

Table 2. Transistor Equivalent Impedance

Transistor State	R_p	C_p	X_p
On	52.5 Ω	6.01 fF	-441 Ω
Off	2.4 k Ω	9.7 fF	-272 Ω

When the transistor is off, the model adds about a 3° phase shift to each path. Because this phase is consistent in each leg it will not show up in the electrically synthesized beam pattern, only the relative phase plays a role. The plot in Figure 33 addresses the matching when looking into the antenna crossover feed lines from Butler Matrix. When the output is terminated with exactly 50Ω and the transistor is off the return loss is 32.3dB compared to when the pads are open and the transistor is on, 14.9dB.

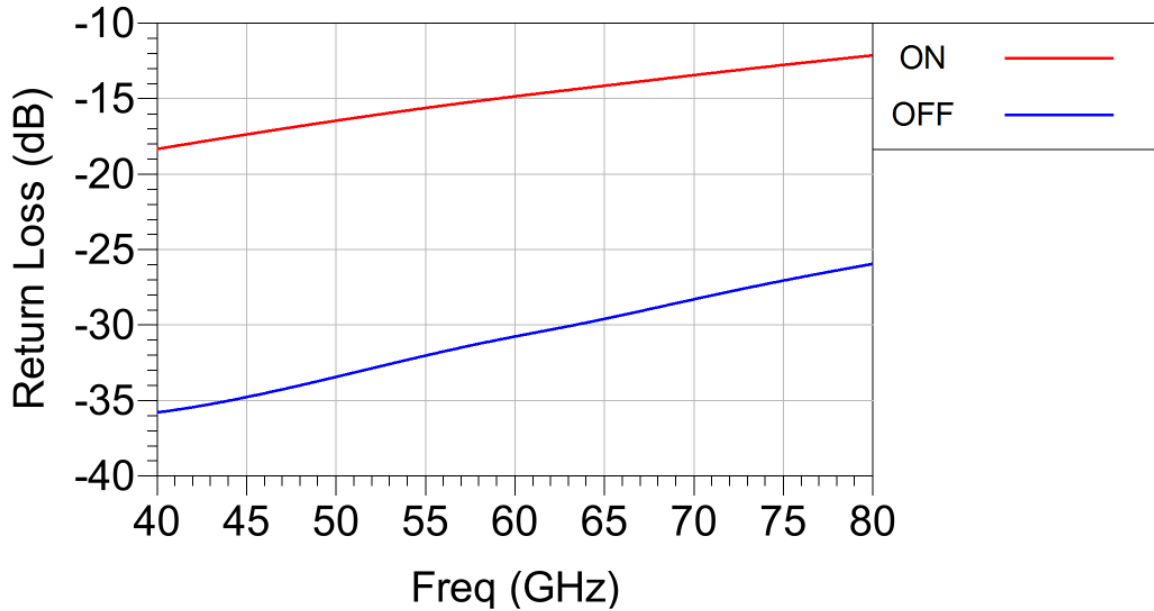


Figure 33. Effects of transistor in output matching.

Antenna Array

To complete the design a basic antenna array has been incorporated into the design to show how the Butler Matrix combined performance. The designer makes attempts to be practical by following design requirements for an Alumina substrate available from Nanowave’s website [15]. The design of the antenna begins at the bond pads continues through flip chip bonding, routing, and finishes at the antennas.

Flip Chip Bonding

The interconnect between the antenna substrate is made using flip chip bonding. The design uses a 40µm gold ball bond compressed to 25µm height between the pads of the IC and antenna substrate. Simulation shows between 10 and 15dB of return loss looking from the IC and antenna, respectively, and a simulated insertion loss of ~0.44dB, between the IC and antenna substrate at 60 GHz.

In comparison to the alternative method of wire bonding, flip chip offers a bonding solution with a much lower inductance between the silicon IC and the antenna substrate. Wire bonding inductance becomes very difficult to match at high frequency and requires addition of parallel capacitance to form a matching network. These capacitances in parallel take extra space, space that is not available due to the tight layout of the signals lines on the IC. For this reason, it was favorable to use coplanar waveguides to reduce the coupling between the adjacent traces. The ground traces separating the signals lines served to bring the isolation between traces to less than -20dB between any path. The CPW was also used to limit the design to a single plane. In reference to the Nanowave process, [15], the vias would have been relatively large in comparison to the transmission lines. Because of the 100 μm GSG pitch, vias could not be placed between signals line without violating the spacing requirements. Using a CPW transmission line allows for the adjustment of ground spacing and trace width to match trace impedance. The signal trace measures 65 μm in width with 40 μm spacing between the signal and ground traces.

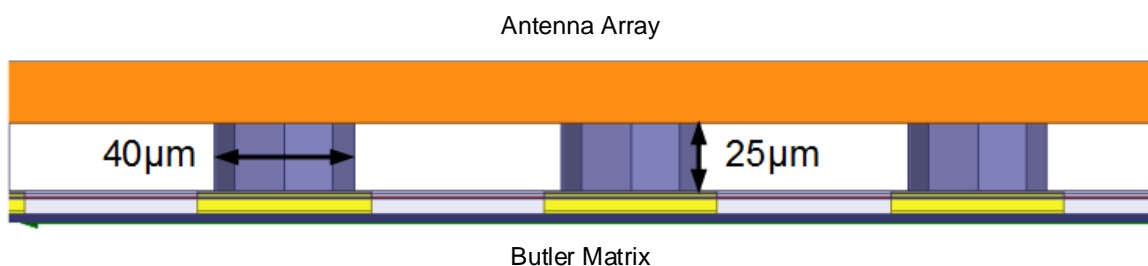


Figure 34. Flip chip wire bond side view used between Butler Matrix and antenna array.

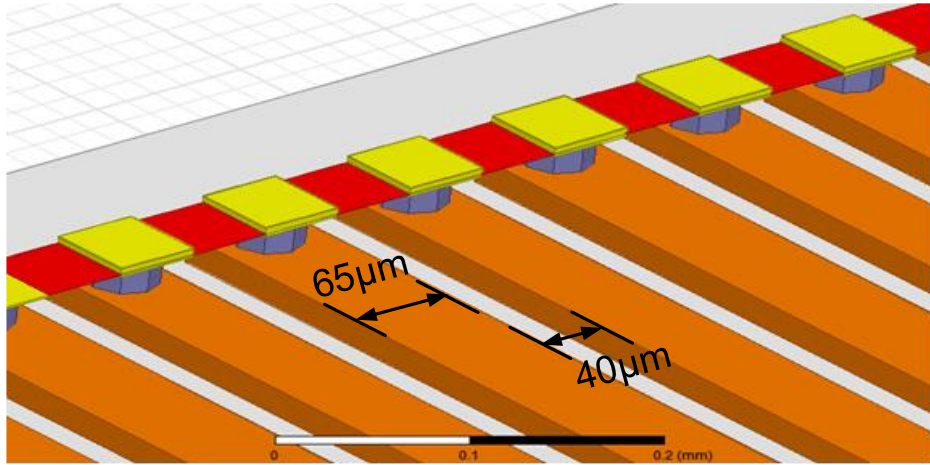


Figure 35. Flip chip wire bonds between silicon IC and antenna substrate.

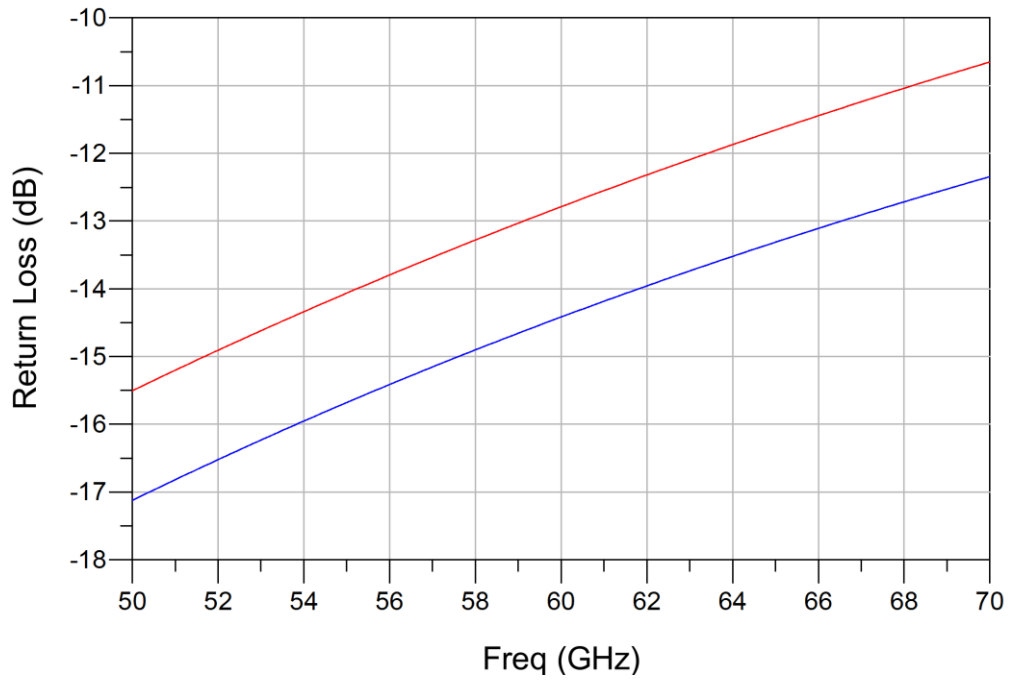


Figure 36. Flip chip matching between the silicon IC and antenna feed lines.

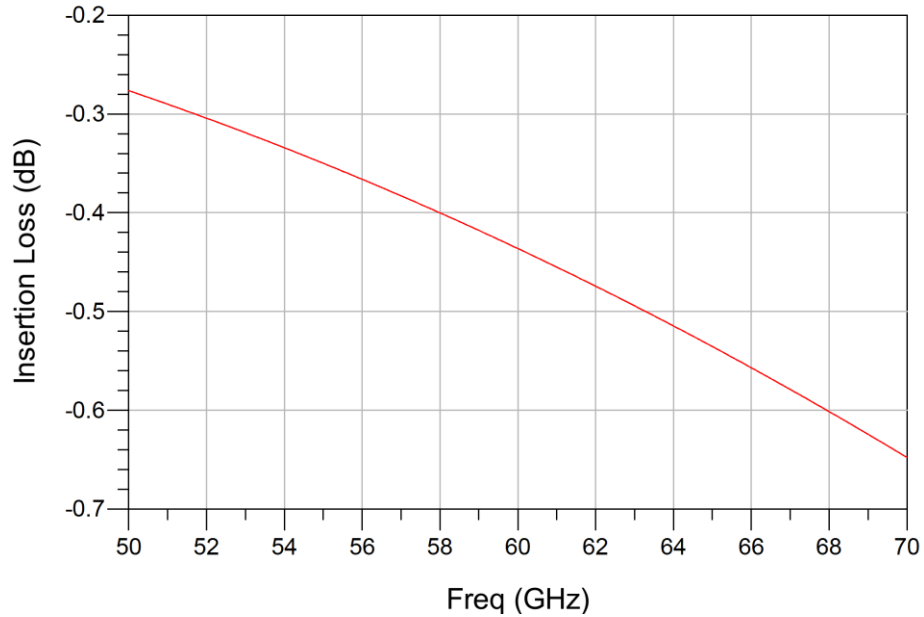


Figure 37. Insertion loss of the flip chip bonds.

Antenna Feed Lines

Antenna feed lines serve to maintain signal phase between the applied signals. For the sake of simplicity and due to the design rules of the Nanowave process, the design of the antennas and feed lines were kept planar. The traces on the outside set the phase delay. These traces cannot be shortened thus the rest of the traces must lengthen to match this electrical distance. By using meander lines the phase delays are matched within 2° at 60GHz. Because these feed lines are the same physical length, the relative phase is matched across frequency.

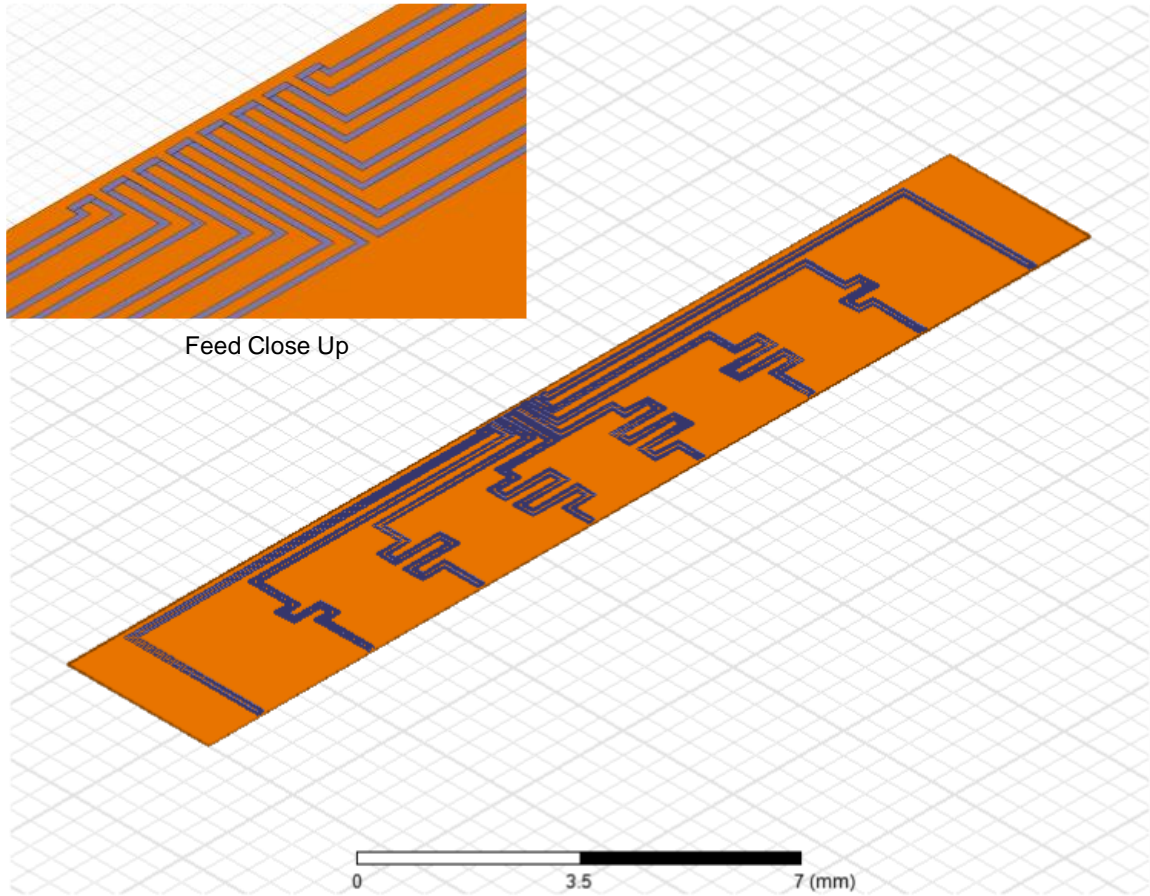


Figure 38. EM model for the antenna feed structure.

Ideally the coupling should be as low as possible to reduce errors in phase and amplitude. The coupling between all paths was simulated less than -23dB .

Antenna Array

The flip chip bonding and tight spacing between feed traces prompted the antenna feed network to be planar. To maintain this planar structure the antenna array uses slot dipole antennas. Although inherently narrowband, it allows the antennas to be fed directly from the CPW.

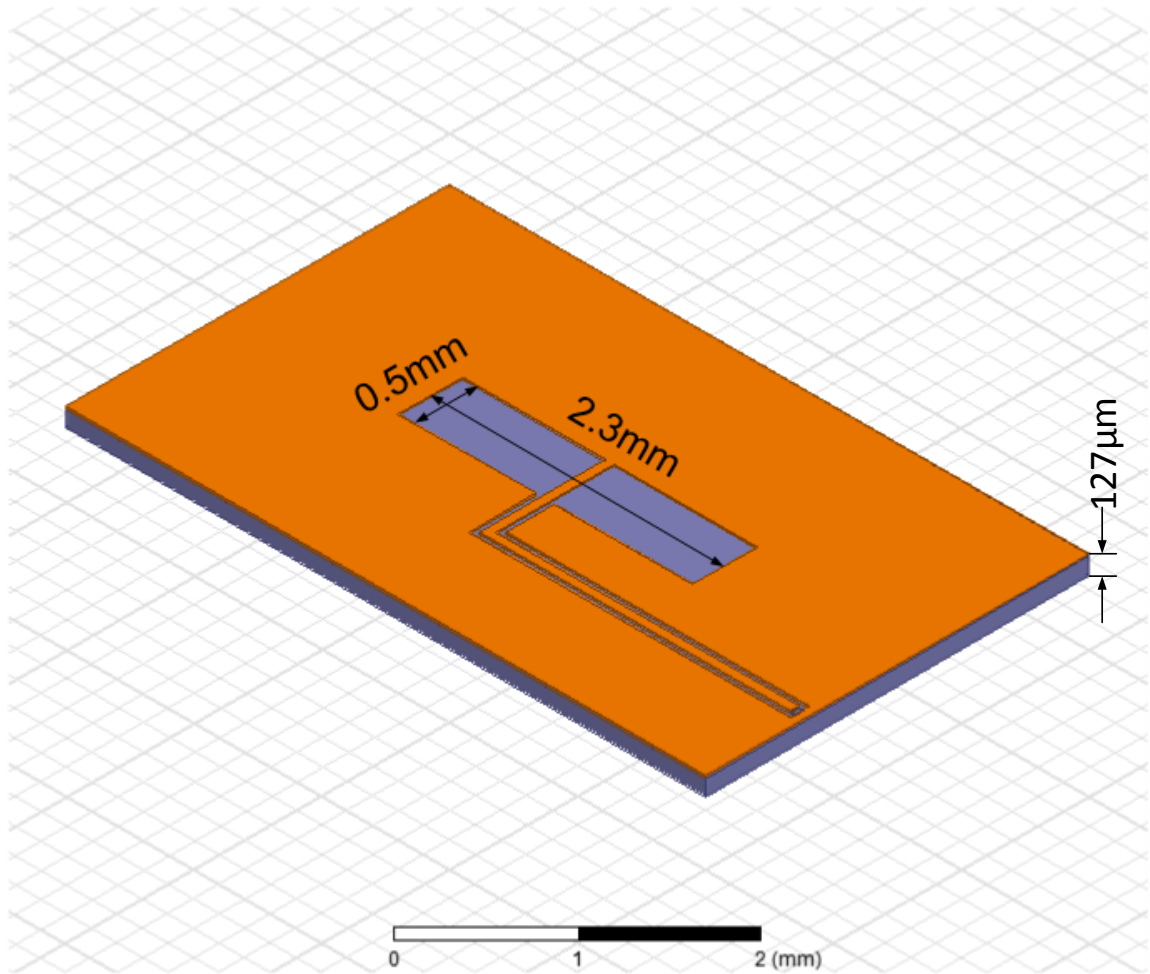


Figure 39. Single slot dipole and associated dimensions.

To create the 8 element antenna array, the slot dipoles were spaced at a distance of $\lambda/2$, Figure 40. These elements were then feed by an S-parameter block of the Butler Matrix connected to the S-parameter block of the flip chip bonds loaded by the impedance of the antenna array. These provided the signals to stimulate the feed network and generate the radiation patterns.

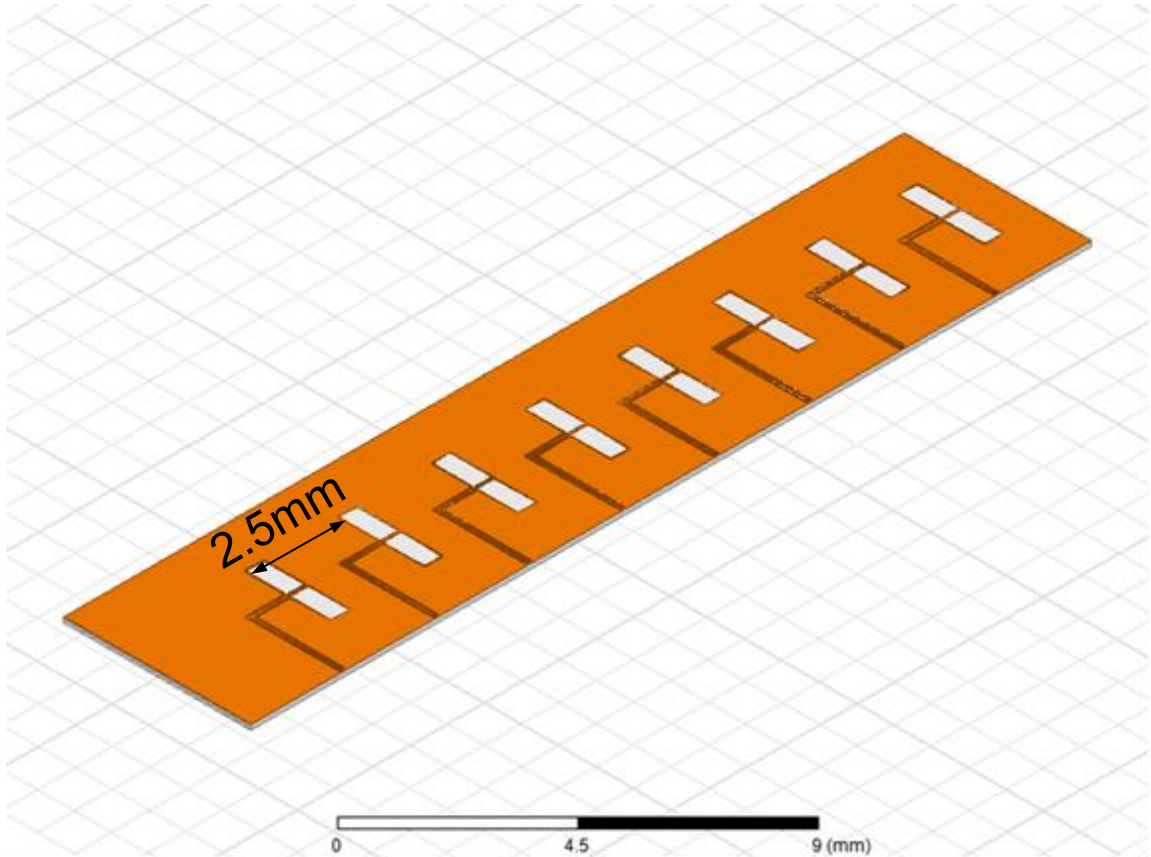


Figure 40. 8 element linear array.

Chapter 4

Simulation Results

The Butler Matrix and components were designed and simulated in a HFSS®, a full 3D EM simulator to create the electrically synthesized beam pattern. The radiation patterns that follow use an S-parameter characterization of the Butler Matrix and flip chip bonds to feed the antenna array.

To simulate changes to the incident angle, the phase difference is swept over the range of -180° to 180° , Figure 41. The Butler Matrix response to this signal shows 8 distinct peaks formed at each of the 8 inputs corresponding to 8 unique angles. The average passive insertion loss is $\sim 3.26\text{dB}$ (simulated) at 60GHz . The Butler Matrix here preserves a 15dB PNR from 57GHz – 63GHz . If the PNR is relaxed to 10dB the bandwidth expands from 49.2GHz to 70.7GHz .

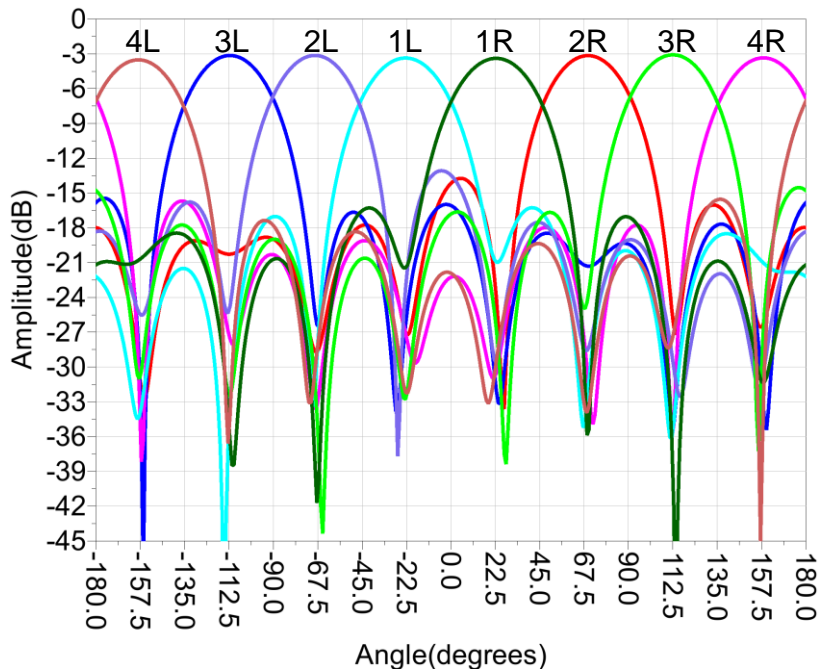


Figure 41. Simulated electrically synthesized beam pattern.

Table 3. Peak to Null Ratio for Excited Beams

Beam	IL	PNR
4L	3.5dB	17.2dB
3L	3.15dB	17.1dB
2L	3.12dB	23.38dB
1L	3.35dB	18.05dB
1R	3.4dB	17.5dB
2R	3.15dB	18.05dB
3R	3.08dB	22.72dB
4R	3.35dB	17.35dB

Plots of PNR with respect to frequency yield frequency dependent performance. The plots formed are fixed at peak angles established in the synthesized beam plot and are swept across frequency. In each plot, only one channel is active while all others are rejected by the cancellation property of the Butler Matrix. While four plots are presented, at most two channels can be responsible for the upper and lower limit on PNR performance. For a 10dB PNR the lower frequency bound, 49.2GHz, is set by the beams formed from inputs 4R/4L. The upper bound, 70.7GHz is set by beams 1R/1L.

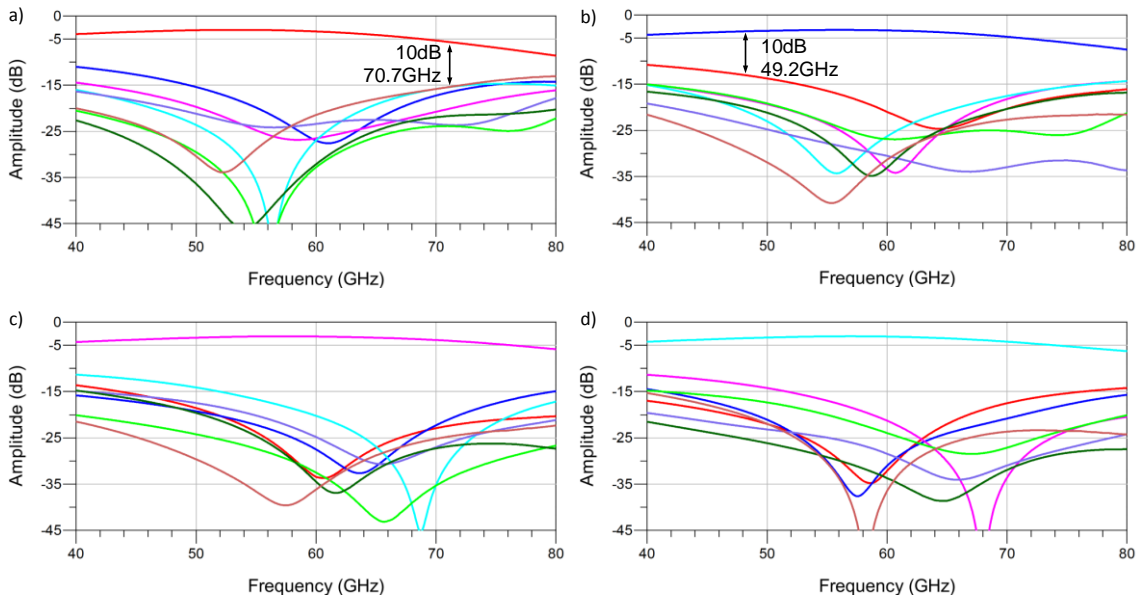


Figure 42. Simulated PNR vs. frequency.

Table 4. Performance Comparison

	[17]	[18]	[19]	This Work
f_0	5.5 GHz	61 GHz	63 GHz	60 GHz
Order	8x8	8x8	4x4	8x8
Dimension	2.5x1.9mm ²	1.45x0.93mm ²	0.335x0.215 mm ²	0.82x0.93mm ²
Matrix IL	3.5dB	3.1dB	2.77dB	3.26dB
Crossover	No	Yes	Yes	Yes

Antenna Array Simulations

The final component of a beam forming network is the antenna array. There are multiple ways antennas can limit the functionality of the beam forming network. The antenna should ideally operate over the frequency range of network and should have near constant directivity over the range of scan angles. The work here used a slot dipole for to allow for connection to a CPW transmission line. The radiation pattern for this single element is shown below in Figure 43. The pattern has a 3dB beam width of 80°. As a result the beams beyond a scan angle of 40° exhibit lower gain than those within the half power beam width. For an 8×8 Butler Matrix Table 5 shows array performance for single element excitation.

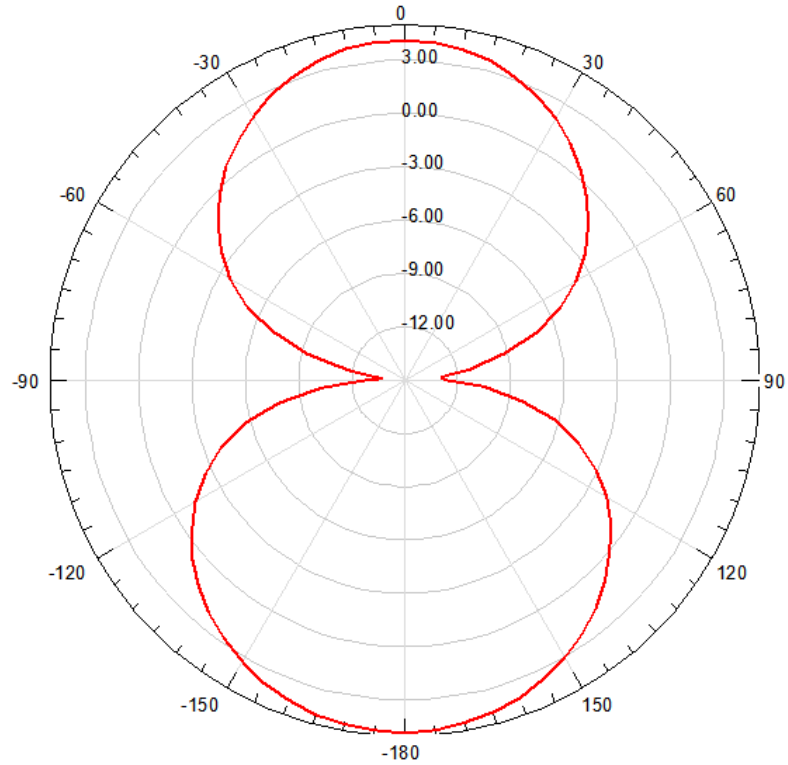


Figure 43. Slot dipole radiation pattern.

Table 5. Simulated electrically synthesized beam and antenna pattern performance.

Excited Beam	Simulated Phase Difference	Theoretical Scan Angle	Simulated Scan Angle	Side Lobe Level	Gain
4L	-158.5°	-61.70°	-56°	-8.1dBc	10.00dB
3L	-112.1°	-38.52°	-37°	-11.43dBc	11.00dB
2L	-69.0°	-22.54°	-22°	-9.45dBc	11.17dB
1L	-23.1°	-7.37°	-6°	-12.74dBc	12.09dB
1R	22.9°	7.31°	7°	-12.88dBc	12.27dB
2R	69.5°	22.71°	23°	-9.55dBc	11.92dB
3R	112.5°	38.68°	36°	-9.65dBc	11.09dB
4R	158.4°	61.64°	57°	-10.92dB	11.34dB

By exciting two inputs simultaneously with the appropriate phase shift, two adjacent beams create a cosine amplitude taper on the array. This results of these combined excitations are shown in Table 6 and the patterns in appendix A. The gain of the array decreases during combination but the side lobe levels improve.

Table 6. Array performance with multiple excitations

Beam Combination	Scan Angle	Gain	Side Lobe Level
4R and 3R	-45°	7.36dB	-12.56dBc
3R and 2R	-30°	7.87dB	-16.16dBc
2R and 1R	-16°	7.57dB	-15.41dBc
1R and 1L	0°	8.94dB	-18.23dBc
1L and 2L	17°	8.29dB	-15.01dBc
2L and 3L	30°	8.75dB	-15.94dBc
3L and 4L	45°	8.01dB	-12.76dBc

Although the Butler Matrix shows a loss of about 3.26dB on average, this loss is made up through the gain from the antenna array. The following figures Figure 44 - Figure 51 show the radiation patterns for single port excitation of the Butler Matrix.

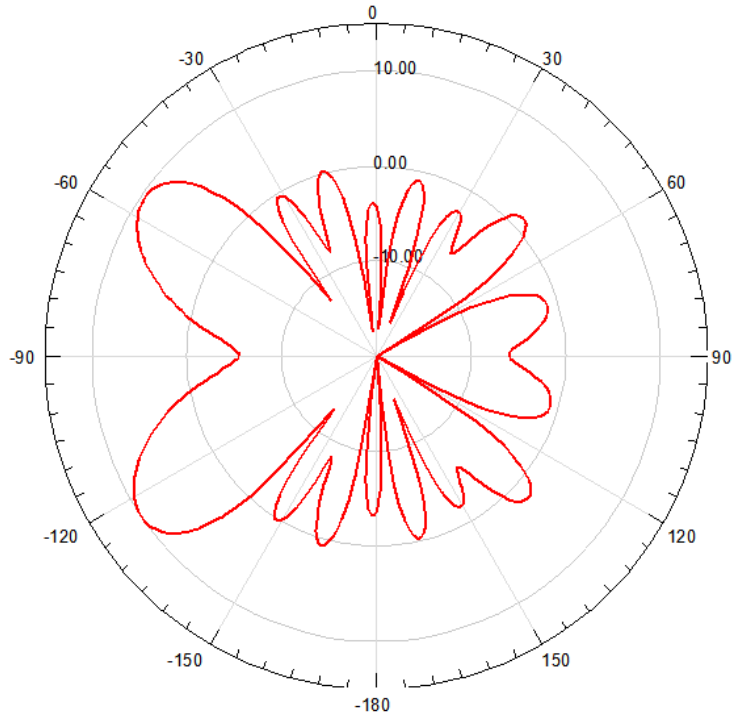


Figure 44. Normalized simulated beam pattern of excitation 4L.

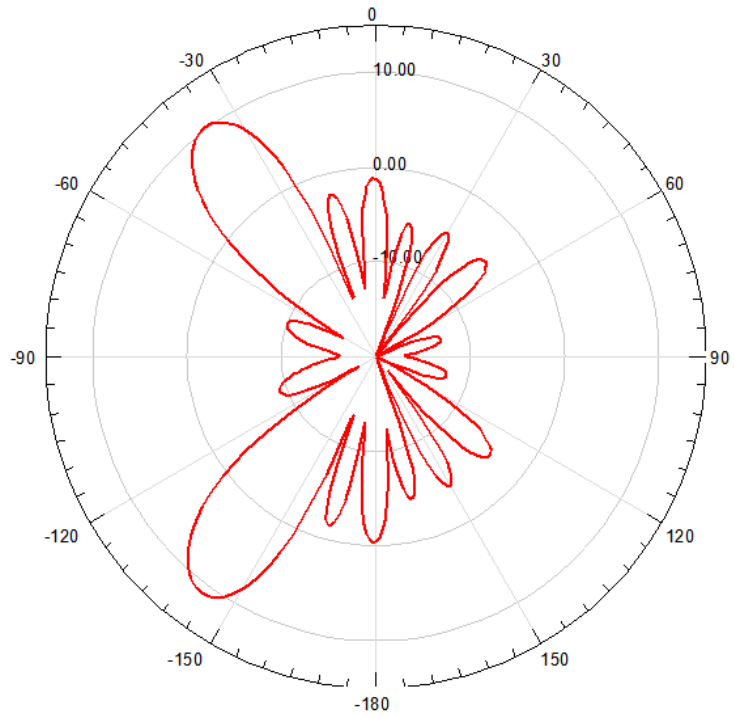


Figure 45. Normalized simulated beam pattern of excitation 3L.

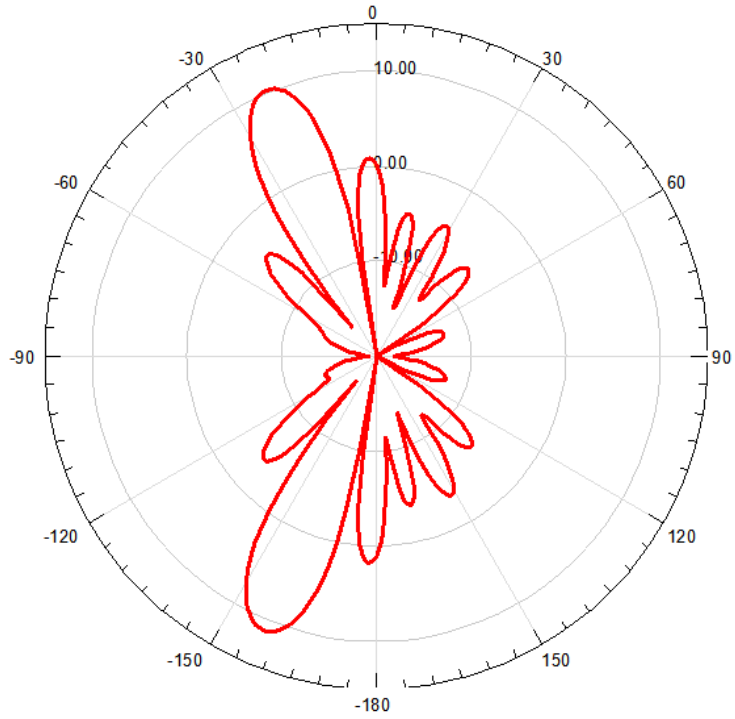


Figure 46. Normalized simulated beam pattern of excitation 2L.

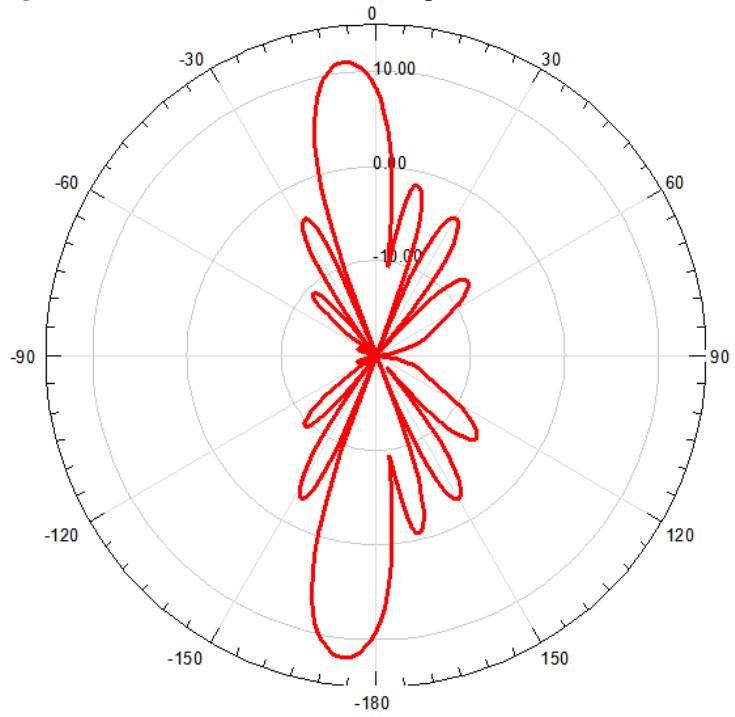


Figure 47. Normalized simulated beam pattern of excitation 1L.

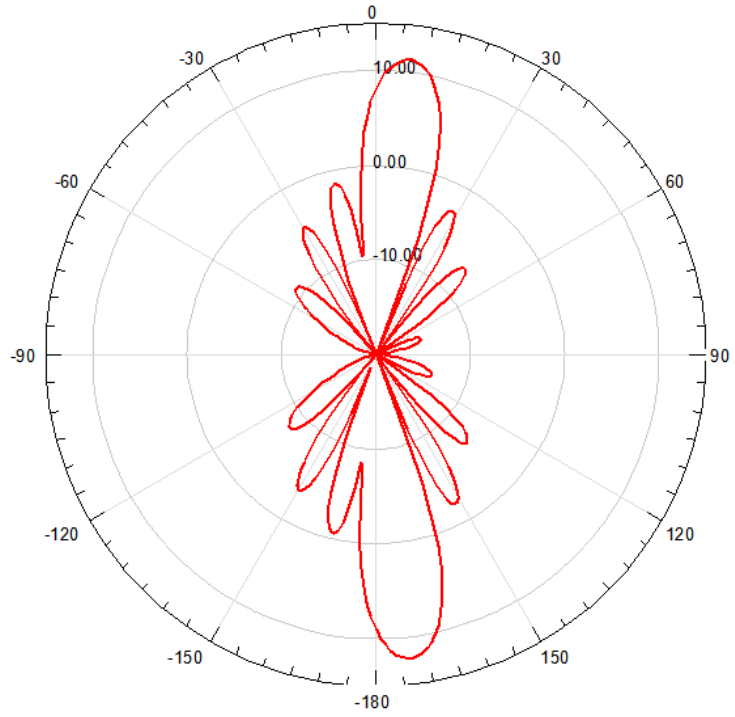


Figure 48. Normalized simulated beam pattern of excitation 1R.

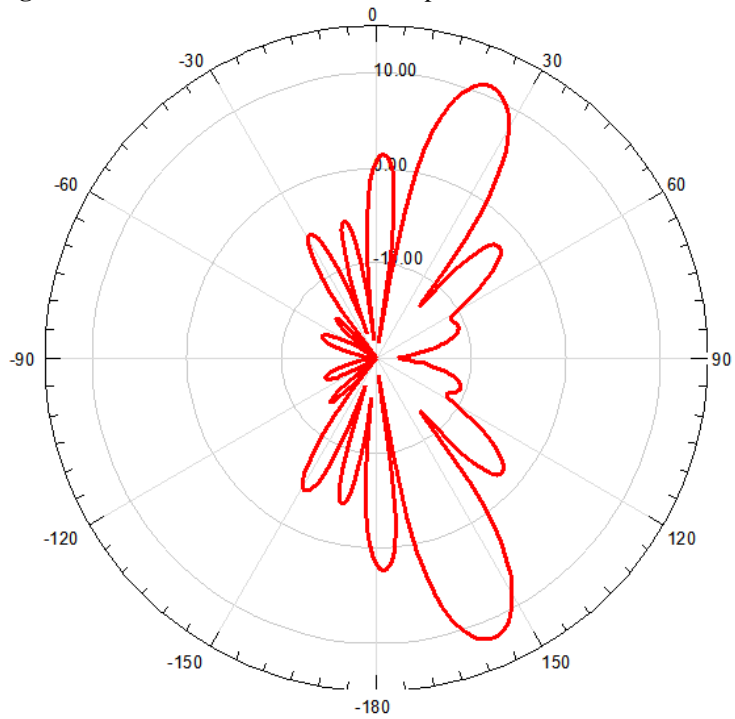


Figure 49. Normalized simulated beam pattern of excitation 2R.

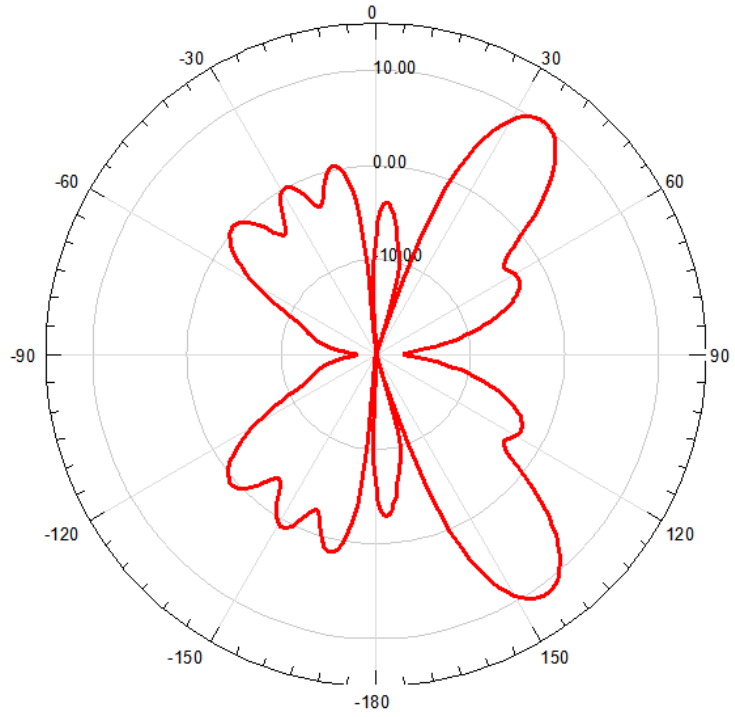


Figure 50. Normalized simulated beam pattern of excitation 3R.

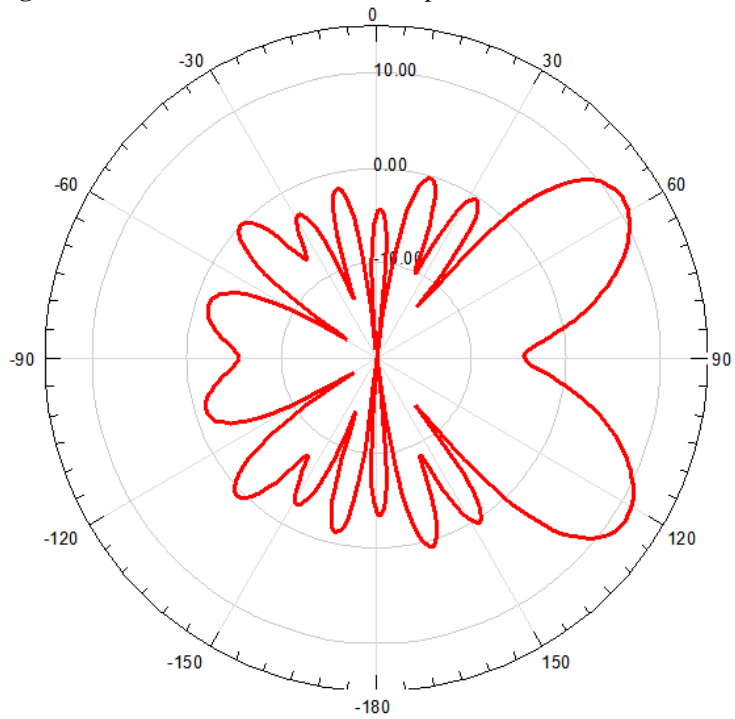


Figure 51. Normalized simulated beam pattern of excitation 4R.

Chapter 5

Conclusion and Future Work

By leveraging a transformer based coupler, the core element of the Butler Matrix, the size was able to be substantially reduced. Instead of being limited by the dimensions of the coupler, the overall size is limited by the pads. This is especially necessary in higher order Butler Matrices as the size more than doubles with order. This reduction in size enables the technology to be integrated using a standard 65nm Bulk CMOS process.

In driving the size of the Butler Matrix down, several tradeoffs were made during the design process. In designing the phase shifters, to reduce size where large phase shifts were needed, π -networks were used. The finite Q of the capacitors significantly impacted the loss of the 67.5° path relative the other paths. Due to this mismatch, there can no longer be perfect cancellation of incoming signals which increases the nulls of the electrically synthesized beam pattern. Transmission sees similar performance tradeoffs in the nulls and side lobes of the matrix. To correct this while keeping the matrix passive would mean inserting additional loss in other paths so each path incurs the same amount of loss.

The other pitfall of the compact design is the narrow bandwidth of the phase shifters. While broadband passive phase shifters are available [23] and [24], the relative size would overshadow the desired size reduction. Moreover, to implement broadband phase performance, the delay of each feed line would need to be equal. Therefore, as frequency changed, the phase delay of each feed line would change by equal amounts. The phase

differences of 22.5° , 45° , 67.5° required by each path would then be implemented using a broadband phase shifter.

The other main limitation on the performance is the transformer based coupler amplitude balance. The coupler exhibits a high pass and low pass relationship between the *Thru* and *Couple* paths causing the single frequency amplitude balance crossover. A method to overcome this limitation has been demonstrated in [25]. The tradeoff here is increased passive loss and area consumed.

Design trade-offs were made to shrink the Butler matrix size for fully on-chip integration, mostly at the expense of Butler matrix performance. However, the matrix exhibits proper beam forming capability and to the knowledge of the author, the Butler Matrix presented has the smallest core area in literature and competitive insertion loss performance among reported 60GHz Butler matrix designs. By limiting the design to such a small form factor the doors are opened to pursue higher order Butler Matrices without overwhelming size.

Appendix A

Combined Radiation Patterns

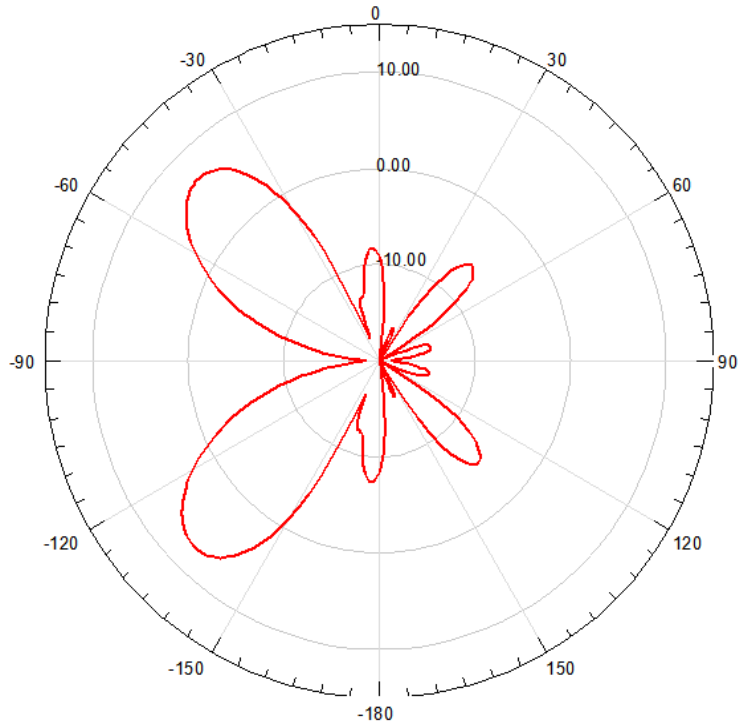


Figure 52. 4R and 3R excitation.

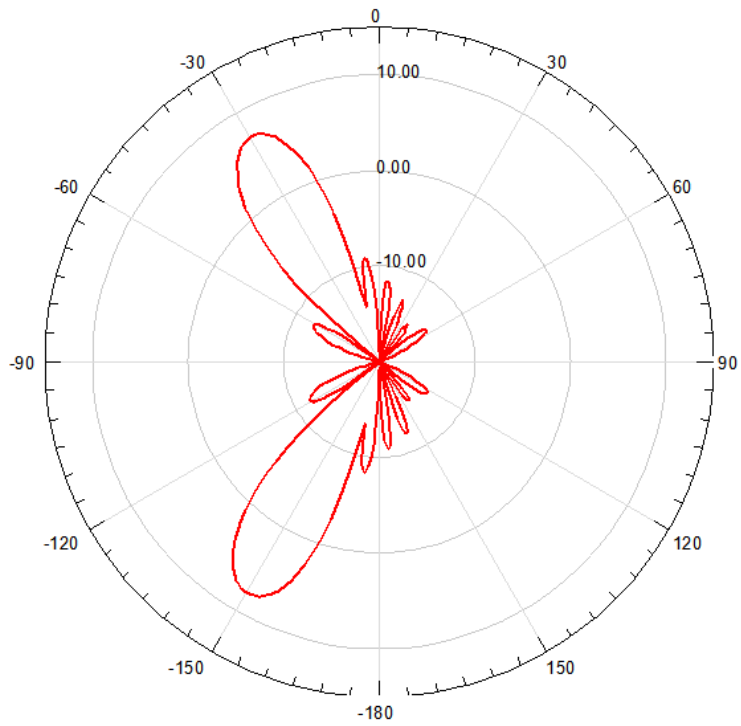


Figure 53. 3R and 2R excitation.

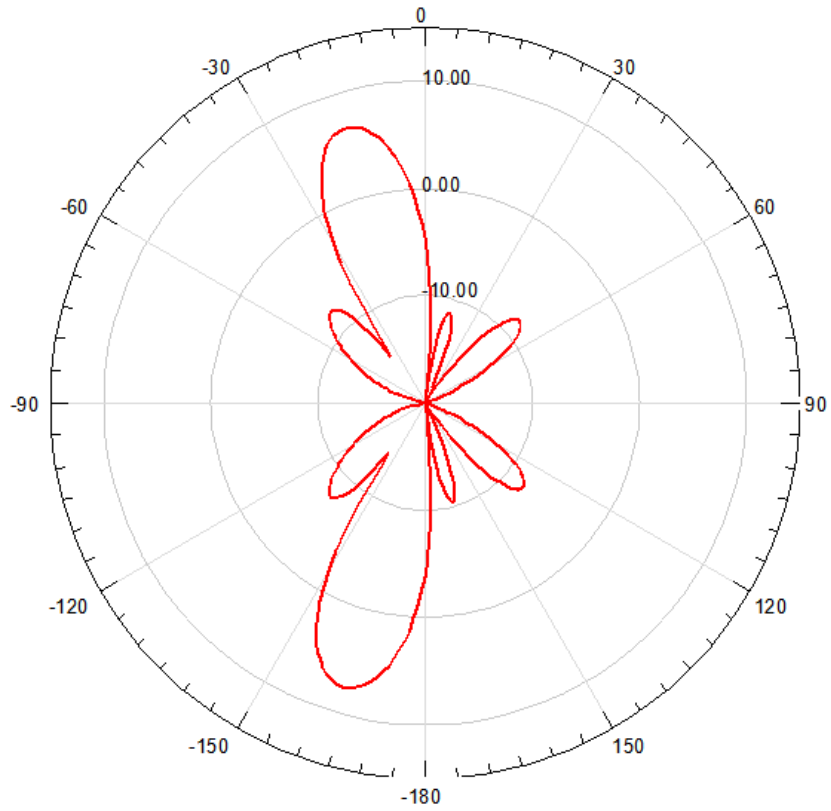


Figure 54. 2R and 1R excitation.

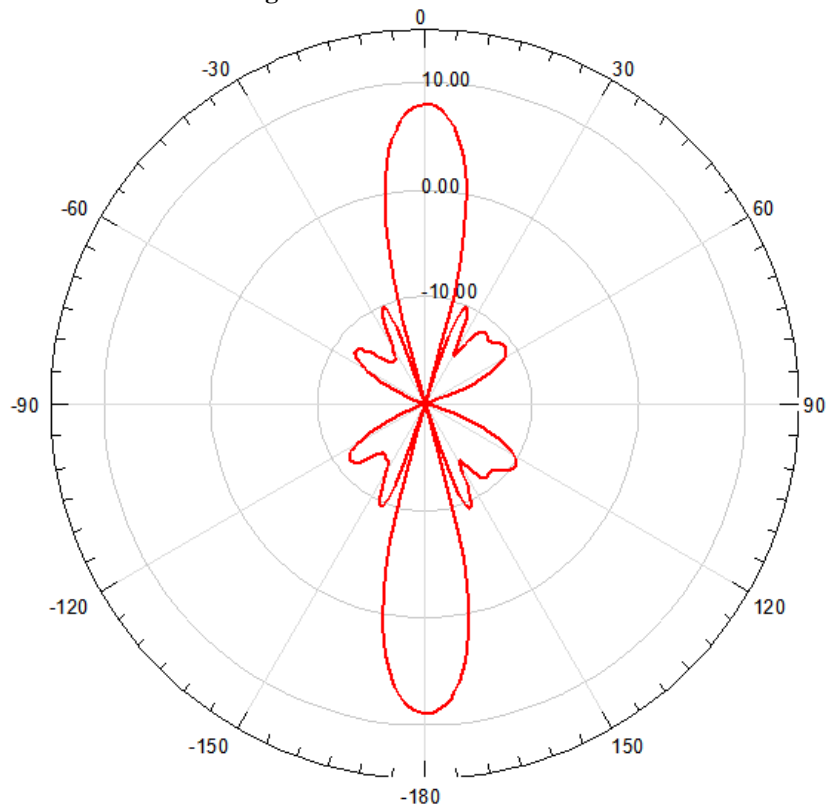


Figure 55. 1R and 1L excitation.

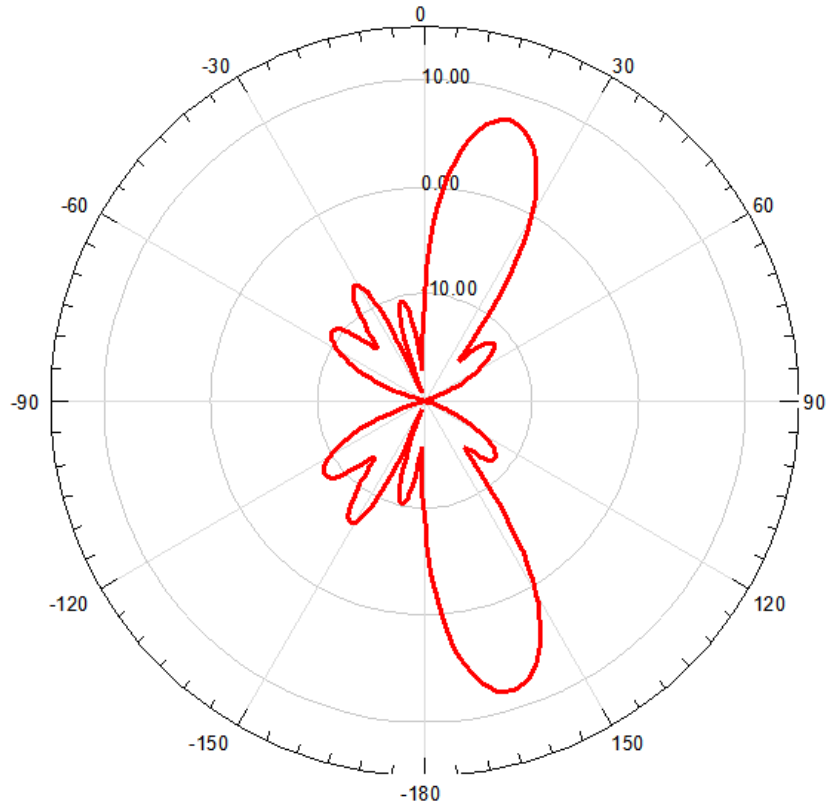


Figure 56. 1R and 2R excitation.

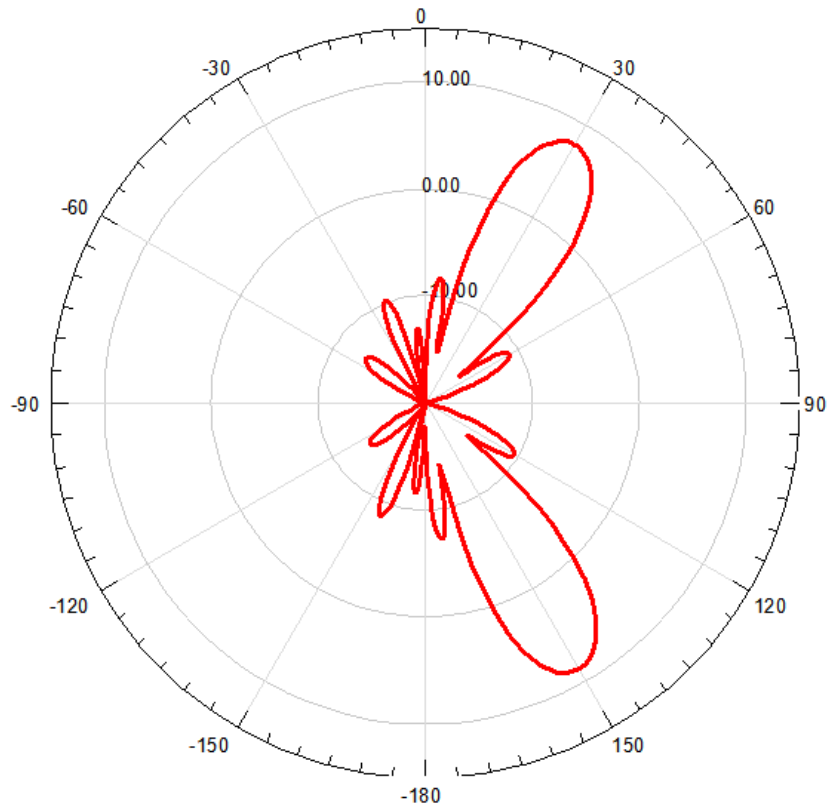


Figure 57. 2R and 3R excitation.

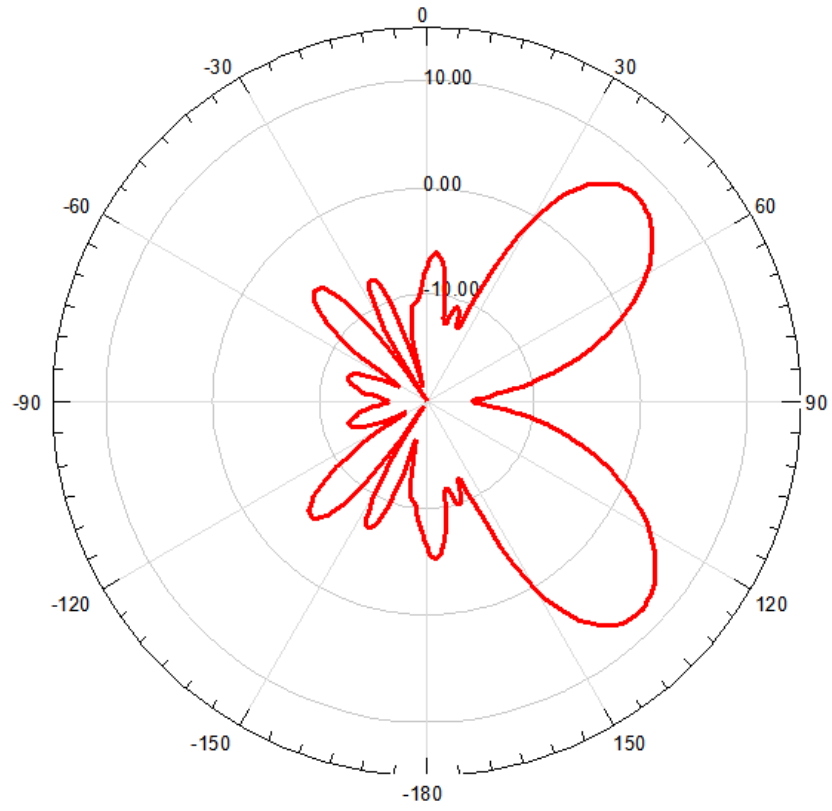


Figure 58. 3R and 4R excitation.

References

- [1] Gtri.gatech.edu, 'Phased-Array Radar: GTRI Supports Test and Evaluation of Next Generation Jammer | Georgia Tech Research Institute', 2015. [Online]. Available: <http://www.gtri.gatech.edu/casestudy/phased-array-radar>.
- [2] 'Aerospace System Improvements Enabled By Modern Phased Array Radar', 2015. [Online]. Available: <http://www.northropgrumman.com/capabilities/anapg80aesaradar/documents/aesa-whitepaper.pdf>.
- [3] Mailloux, R. J., Phased Array Antenna Handbook. Artech House, 1994.
- [4] Hansen, R. C., Microwave Scanning Antennas. California: Peninsula Publishing, 1985.
- [5] 'WirelessHD Specification Overview', 2010. [Online]. Available: <http://www.wirelesshd.org/pdfs/WirelessHD-Specification-Overview-v1.1May2010.pdf>. [Accessed: 22- Jan- 2015].
- [6] A 60GHz CMOS phased-array transceiver pair for multi-Gb/s wireless communications, ISSCC 2011
- [7] A SiGe BiCMOS 16-element phased-array transmitter for 60GHz communications, ISSCC 2010
- [8] A 16-element phased-array receiver IC for 60-GHz communications in SiGe BiCMOS, RFIC 2010
- [9] A fully-integrated dual-polarization 16-element W-band phased-array transceiver in SiGe BiCMOS, RFIC 2013
- [10] J. Butler and R. Howe, "Beamforming matrix simplifies design of electronically scanned antennas," *Electron. Design*, no. 9, pp. 170–173, Apr. 1961.
- [11] C. A. Balanis, *Antenna Theory: Analysis and Design*, 3rd ed. Hoboken, NJ: Wiley, 2005.
- [12] D. M. Pozar, *Microwave Engineering*, 2nd ed. New York: Wiley, 1998.
- [13] J. S. Park, S. Kousai, and H. Wang, "A Fully Differential Ultra-Compact Broadband Transformer Based Quadrature Generation Scheme," *Custom Integrated Circuits Conference (CICC)*, 2013 IEEE, vol., no., pp.1,4, 22-25 Sept. 2013.

- [14] J.S. Park; T. Chi; H. Wang, "An ultra-broadband compact mm-wave butler matrix in CMOS for array-based MIMO systems," *Custom Integrated Circuits Conference (CICC)*, 2013 IEEE , vol., no., pp.1,4, 22-25 Sept. 2013
- [15] Nanowavetech.com, 'Nanowave Technologies Inc. Expertise in High Power Solid-State Transceivers for Aerospace', 2015. [Online]. Available: http://www.nanowavetech.com/prod_thinfilm.htm.
- [16] Nord, H., "Implementation of 8 x 8 Butler matrix in microstrip," Diploma Thesis, Royal Institute of Technology, Stockholm, 1997.
- [17] B. Cetinoneri, Y. A. Atesal, G.M. Rebeiz, "An 8x8 Butler Matrix in 0.13- μm CMOS for 5–6-GHz Multibeam Applications," *Microwave Theory and Techniques*, IEEE Transactions on , vol.59, no.2, pp.295,301, Feb. 2011.
- [18] T. Y. Chin; J. C. Wu; S. F. Chang; C. C. Chang, "A V-Band 8 \times 8 CMOS Butler Matrix MMIC," *Microwave Theory and Techniques*, IEEE Transactions on , vol.58, no.12, pp.3538,3546, Dec. 2010
- [19] Park, J.S.; Chi, T.; and Wang, H., "An ultra-broadband compact mm-wave butler matrix in CMOS for array-based MIMO systems," *Custom Integrated Circuits Conference (CICC)*, 2013 IEEE. IEEE, 2013.
- [20] Frye, R.C.; Kapur, S.; Melville, R.C., "A 2-GHz quadrature hybrid implemented in CMOS technology," *Solid-State Circuits, IEEE Journal of* , vol.38, no.3, pp.550,555, Mar 2003
- [21] Krems, T.; Haydl, W.; Massler, H.; Rudiger, J., "Millimeter-wave performance of chip interconnections using wire bonding and flip chip," *Microwave Symposium Digest, 1996., IEEE MTT-S International* , vol.1, no., pp.247,250 vol.1, 17-21 June 1996
- [22] Hirose, Tatsuya; Makiyama, K.; Ono, K.; Shimura, T.M.; Aoki, Shigenori; Ohashi, Y.; Yokokawa, S.; Watanabe, Y., "A flip-chip MMIC design with coplanar waveguide transmission line in the W-band," *Microwave Theory and Techniques, IEEE Transactions on* , vol.46, no.12, pp.2276,2282, Dec 1998
- [23] Abbosh, A.M., "Broadband Fixed Phase Shifters," *Microwave and Wireless Components Letters, IEEE* , vol.21, no.1, pp.22,24, Jan. 2011
- [24] Schiffman, B.M., "A New Class of Broad-Band Microwave 90-Degree Phase Shifters," *Microwave Theory and Techniques, IRE Transactions on* , vol.6, no.2, pp.232,237, April 1958
- [25] T-W Li, J. Park, and H. Wang, "An Ultra-broadband 360° Full-Span Transformer-Based Differential Vector Modulator Phase Rotator In CMOS,"to

appear in the Government Microcircuit Applications and Critical Technology Conference (GOMACTech), Mar. 2015.

- [26] S. Lepkowski, J. Park, T. Chi, and H. Wang, "A Transformer Based Ultra-Compact 8×8 Mm-Wave Butler Matrix Fully Integrated in 65nm Bulk CMOS," to appear in the Government Microcircuit Applications and Critical Technology Conference (GOMACTech), Mar. 2015.
- [27] Chin, T. Y.; Wu, J. C.; Chang, S. F.; Chang, C. C., "A V-Band 8×8 CMOS Butler Matrix MMIC," *Microwave Theory and Techniques, IEEE Transactions on* , vol.58, no.12, pp.3538,3546, Dec. 2010
- [28] Wallington, J.R., "Analysis, Design and Performance of a Microstrip Butler Matrix," *Microwave Conference, 1973. 3rd European* , vol.1, no., pp.1,4, 4-7 Sept. 1973
- [29] Fakoukakis, F. E. and Kyriacou, G. A., ", " *Progress In Electromagnetics Research B*, Vol. 51, 33-64, 2013
- [30] Lange, J., "Interdigitated Stripline Quadrature Hybrid (Correspondence)," *Microwave Theory and Techniques, IEEE Transactions on* , vol.17, no.12, pp.1150,1151, Dec 1969
- [31] Laheurte, J.-M.; Katehi, L.P.B.; Rebeiz, G.M., "CPW-fed slot antennas on multilayer dielectric substrates," *Antennas and Propagation, IEEE Transactions on* , vol.44, no.8, pp.1102,1111, Aug 1996
- [32] Liu, H. C.; Horng, T. S.; Alexopoulos, N.G., "Radiation of printed antennas with a coplanar waveguide feed," *Antennas and Propagation, IEEE Transactions on* , vol.43, no.10, pp.1143,1148, Oct 1995
- [33] Nejad, I. V.; Neyestanak, L. A.A.; Shahzadi, A., "Compact broadband quadrature hybrid coupler using planar artificial transmission line," *Electronics Letters* , vol.48, no.25, pp.1602,1603, December 6 2012
- [34] Yamasaki, J.; Ohta, I.; Kawai, T.; Kokubo, Y., "Design of broadband semi-lumped and lumped element quadrature hybrids," *Microwave Symposium Digest, 2005 IEEE MTT-S International* , vol., no., pp.4 pp., 12-17 June 2005
- [35] Zheng, S .Y.; Chan, W. S.; Man, K. F., "Broadband Phase Shifter Using Loaded Transmission Line," *Microwave and Wireless Components Letters, IEEE* , vol.20, no.9, pp.498,500, Sept. 2010

- [36] Okazaki, H.; Hirota, T., "Multilayer MMIC broad-side coupler with a symmetric structure," *Microwave and Guided Wave Letters*, IEEE , vol.7, no.6, pp.145,146, June 1997.
- [37] B. Razavi, *RF microelectronics*. Upper Saddle River, NJ: Prentice Hall, 2012.
- [38] Ansoft Corp., <http://www.ansoft.com>